FY19 Lawrence Livermore National Laboratory Experimental Programs at the Omega Laser Facility

R. F. Heeter,[1] F. Albert,[1] S. J. Ali,[1] L. R. Benedetti,[1] N. Candeias Lemos,[1] H. Chen,[1] F. Coppari,[1] A. Fernandez Pañella,[1] D. E. Fratanduono,[1] M. Ginnane,[2] M. Gorman,[1] M. Hohenberger,[1] S. Jiang,[1] G. E. Kemp,[1] S. F. Khan,[1] P. King,[1] A. Krygier,[1] A. E. Lazicki,[1] T. Ma,[1] M. J. MacDonald,[1] D. Mariscal,[1] E. V. Marley,[1] M. C. Marshall,[1] D. A. Martinez,[1] M. A. Millot,[1] C. A. J. Palmer,[3] H. S. Park,[1] J. Park,[4] G. Perez Callejo,[3] Y. Ping,[1] B. B. Pollock,[1] P. L. Poole,[1] J. Ralph,[1] A. M. Saunders,[1] G. F. Swadling,[1] R. Tommasini,[1] K. Widmann,[1] A. Zylstra,[1] O. L. Landen,1 [1] W. W. Hsing,[1] and A. S. Wan[1]

[1]Lawrence Livermore National Laboratory
[2]Laboratory for Laser Energetics, University of Rochester
[3]Oxford University
[4]University of California, San Diego

In fiscal year 2019 (FY19), Lawrence Livermore National Laboratory's (LLNL's) High-Energy-Density (HED) Physics and Indirect-Drive Inertial Confinement Fusion (ICF-ID) Programs conducted numerous campaigns on the OMEGA and OMEGA EP Laser Systems. This was the 21st year of national laboratory collaborative experiments at the Omega Laser Facility since the Nova Laser at LLNL shut down in 1999 (Ref. 1), building upon prior collaborations. In FY19 overall, these LLNL programs led 465 target shots, with 283 shots using only the OMEGA Laser System, 172 shots using only the OMEGA EP Laser System, and 10 joint shots using both lasers together. Approximately 28% of the total number of shots (60 OMEGA shots and 71 OMEGA EP shots) supported the ICF-ID Campaign. The remaining 72% (223 OMEGA-only shots, 101 OMEGA EP-only shots, and 10 joint shots) were dedicated to experiments for HED physics. Highlights of the various HED and ICF-ID campaigns are summarized in the following reports.

In addition to these experiments, LLNL Principal Investigators (PI's) led a variety of Laboratory Basic Science (LBS) campaigns using OMEGA and OMEGA EP, including 99 target shots using only OMEGA and 39 shots using only OMEGA EP. The highlights of these campaigns are summarized in the LBS section (p. 257).

Overall, LLNL PI's led a total of 603 shots at LLE in FY19. In addition, LLNL PI's supported 47 National Laser Users' Facility (NLUF) shots on OMEGA and 31 NLUF shots on OMEGA EP in collaboration with the academic community.

Indirect-Drive Inertial Confinement Fusion Experiments

Hydrodynamic Response from Nonuniformities in High-Density Carbon Ablators

Principal Investigator: S. Ali

Co-investigators: P. M. Celliers, A. Fernandez Pañella, C. Weber, S. W. Haan, and V. A. Smalyuk

Performance and yield from fusion capsules at the National Ignition Facility (NIF) are highly dependent on the uniformity of the capsule implosion. Hydrodynamic instabilities are a significant source of performance degradation during the implosion and can arise from, among other reasons, intrinsic heterogeneity within the capsule material. High-density carbon (HDC) is a polycrystalline diamond material that has a complex microstructure, as well as being acoustically anisotropic, which can lead to variations in the shock speed in crystallites of different orientations, potentially seeding instabilities. Additional sources of heterogeneous response include the behavior of the grain boundary material, which is often of a different bonding character than the crystallites, voids in the deposited material, and static internal stresses in the polycrystalline structure. The current strategy for reducing the impact of internal heterogeneities is to fully melt the ablator material on the first shock, requiring >12 Mbar for HDC.[2–4] This strong shock also raises the entropy of the fuel, making it more difficult to reach the high densities required for ignition. As part of the effort to understand both the origin and impact of the velocity nonuniformities in HDC, we have conducted 2-D velocimetry experiments on planar foils under conditions near the first shock in HDC.

The goal of the Capseed Campaign is to measure shock-front velocity nonuniformities in ICF ablator materials and quantify the level of nonuniformity caused by intrinsic effects. This is done by using the OMEGA high-resolution velocimeter (OHRV) to obtain velocity maps of the optically reflecting shock front following release of the ablator material into either PMMA for the warm experiments or cryogenic deuterium for the cryo experiments. As part of our attempt to move toward more capsule-like targets, as opposed to the planar foils that have been used for past Capseed Campaigns, we have been moving toward using large-diameter (4.5 to 5 mm) capsules for our two half-day campaigns in FY19. Unfortunately, due to the complexity involved in fabricating these large spheres, the 5-mm HDC spheres were not complete in time for 19B, but a secondary goal of measuring the effect of grain size on the nonuniformity was achieved. Relative to the microcrystalline HDC, the onset of velocity uniformity in the 10- to 20-m/s range occurred at just under 10 Mbar, as shown in Fig. 1. This suggests that nanocrystalline capsules can be driven on a lower adiabat than larger grain size capsules while still remaining relatively free of instabilities. This work is ongoing, and target fabrication has made great strides in fabricating the larger-diameter spheres, so the plan remains to move toward the capsule-like samples while still investigating other potential sources of perturbation.

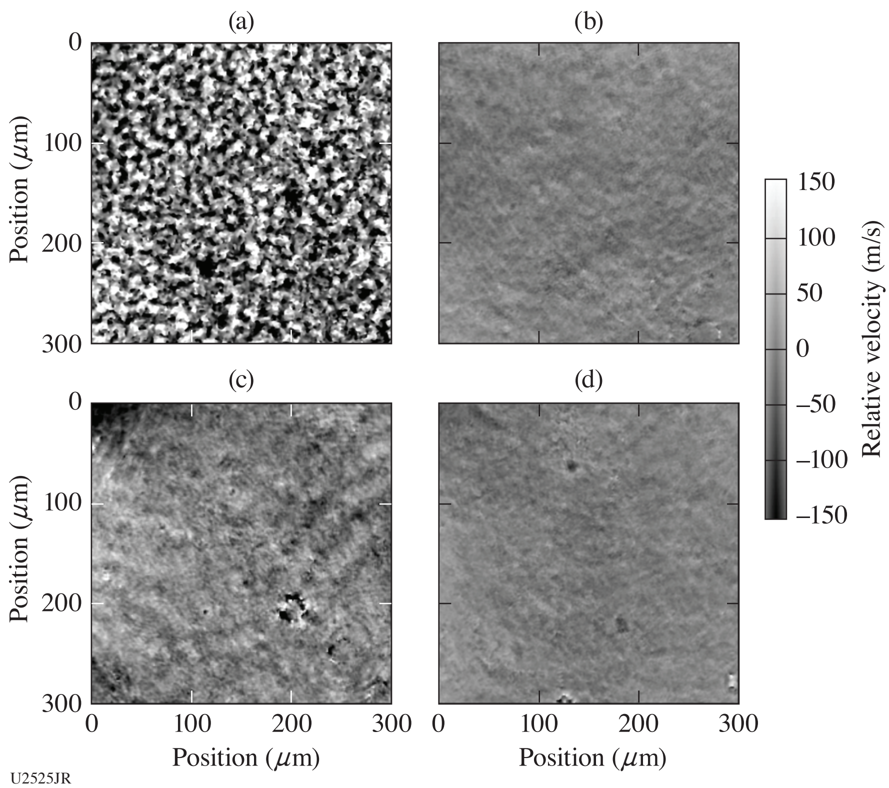

Figure 1
Velocity maps from nanocrystalline HDC releasing into cryogenic D_2 at (a) ~7 Mbar with rms 100 m/s, (b) ~8 to 9 Mbar with rms 45 m/s, (c) ~10 Mbar with rms 14 m/s, and (d) ~12 Mbar with rms 12 m/s. The diagnostic detection limit is 10 m/s for (b) and 5 m/s for (a), (c), and (d).

Determination of EOS and Melt Line of W-Doped Diamond Between 6 and 12 Mbar
Principal Investigator: A. Fernandez Pañella
Co-investigators: M. Millot and P. M. Celliers

This half day on OMEGA EP was designed to collect high-quality data on the melt line and equation of state (EOS) of W-doped diamond (0.3 at. %) in the multi-Mbar range. W-doped HDC is used in ICF capsules on the NIF, but only a scarce amount of EOS data is available, and little is known about what effect the doping has on the diamond melt line. Molecular dynamics (MD) simulations by S. Bonev predict that the melt temperature of HDC decreases with increasing Si dopant concentration. Similar effects are expected with W dopant, but experimental verification is required.

The W-doped HDC-19A Campaign used planar targets and a direct-drive configuration with a Be ablator, a quartz pusher, and two samples side by side: one being W-doped HDC and pure HDC glued together and the other being a quartz witness (see Fig. 2). The velocity profiles were recorded using VISAR (velocity interferometer for any reflector) and the emissivity using SOP (streaked optical pyrometry) (see Fig. 3). Throughout the day, the laser drive energy was changed to probe different shocked pressure states in the diamond.

We obtained six good data points from 600 to 1200 GPa. The experimental design was successful, and shocks were steady, as indicated by the quartz witness velocity history. The W-doped HDC target at 0.3 at. % is completely opaque at the VISAR

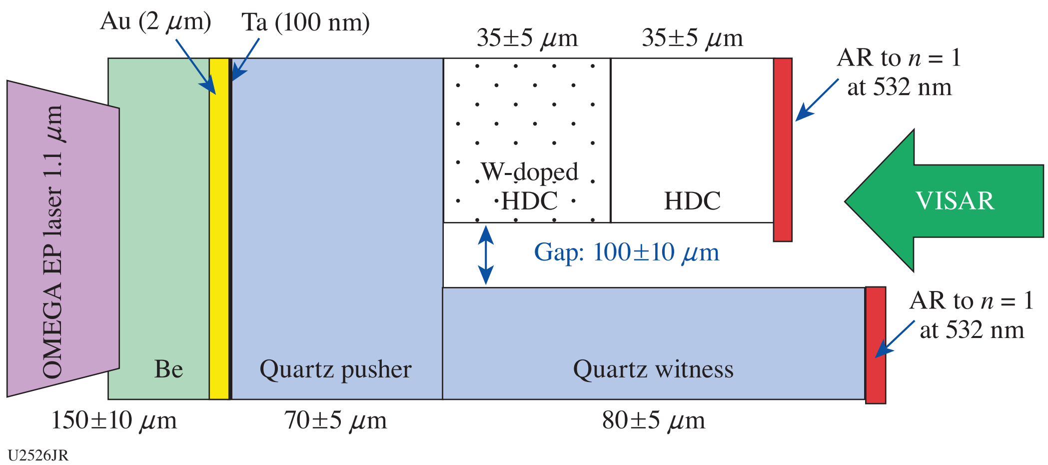

Figure 2
Experimental setup and target design for the W-doped HDC-19A Campaign.

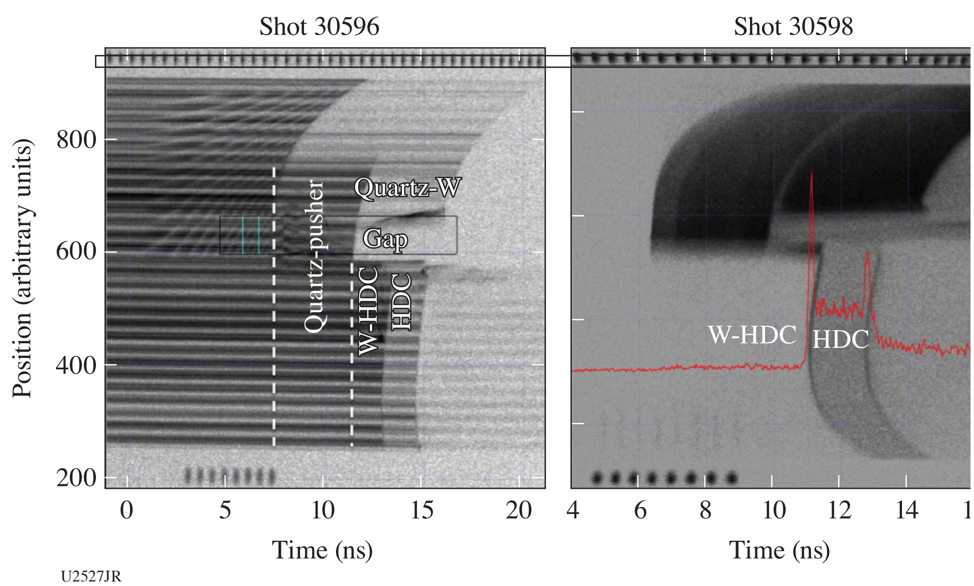

Figure 3
VISAR and SOP data from shot 30596, corresponding to 9.5 Mbar. Neither fringe movement nor emission is observed in the W-HDC sample.

and SOP wavelengths. Transit time analysis will be used to infer EOS data. Furthermore, we will also use the SOP data from the pure and transparent HDC to constrain its temperature along the melt line of pure diamond. Once the data are analyzed, we will be able to constrain the EOS of W-doped HDC in a pressure range relevant for ICF experiments.

Study of the Melting Temperature of Diamond with Pyrometry
Principal Investigator: M. Millot
Co-investigator: P. M. Celliers

This series of shots aims at measuring the shock temperature of diamond over a broad pressure range from 5 Mbar to 40 Mbar. To do this, the approach builds on the previous work by Eggert *et al.* carried out on OMEGA in 2005–2006 and reported in Ref. 5. Namely, the idea is to launch a strong, unsupported shock in a thick sample of diamond and track simultaneously the shock velocity and reflectivity with a VISAR velocimetry instrument [active shock breakout (ASBO)] and the spectral radiance with the SOP.[6] A gray-body approximation using the measured reflectivity to determine the emissivity then allows one to obtain the variation of the shock temperature as a function of shock velocity, which one can relate to pressure using a previously determined U_S–u_p equation-of-state relationship.

With excellent laser performance and support, we collected eight system shots in the half-day allocation, returning excellent-quality data. In particular, the new optical telescope with improved achromaticity and therefore enhanced spatial resolution resulted in noticeably higher-quality SOP (see Fig. 4).

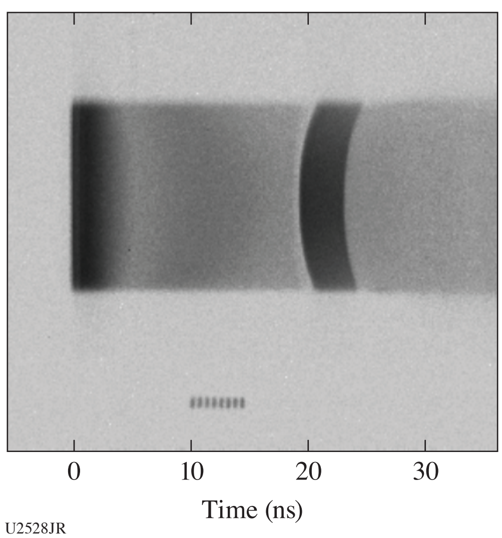

Figure 4
Example SOP data for the Diamond Melt 19A Campaign.

The ongoing data analysis will be used to improve our understanding of the thermodynamic properties of diamond near the pressure–temperature conditions that are relevant for ICF experiments using HDC ablators.[7]

Investigation of the Atomic Structure of Dense Carbon with X-Ray Diffraction
Principal Investigator: M. Millot
Co-investigators: F. Coppari, A. Fernandez Pañella, J. Emig, V. Rekow, and P. M. Celliers

This series of shots aims at measuring the atomic structure of diamond in the multi-megabar range and near the pressure–temperature conditions achieved during the initial stage of ICF implosions using HDC ablators on the NIF.[7] In particular, we aim to unravel how shock-compressed diamond transforms to a conducting fluid above 11 Mbar as expected from previous experiments, numerical simulations, and theoretical modeling. Further, we hope to elucidate if dense fluid carbon formed by shock compression could solidify upon decompression and the link with a possible maximum in the melting curve of carbon near 5 Mbar (Ref. 8).

This campaign on OMEGA EP used a combination of ultrafast x-ray diffraction and optical diagnostics using new laser dynamic compression techniques. We collected excellent-quality data on eight system shots using one UV beam to compress the water sample layer and three UV beams to generate an x-ray source flash for the x-ray diffraction measurement. Preliminary analysis suggests that we successfully managed to record high-quality x-ray diffraction data (see Fig. 5) and scan a broad range of pressure from 5 to 12 Mbar.

The ongoing data analysis and upcoming experiments on OMEGA EP in FY20 and on the NIF will be used to improve our understanding of the microscopic and thermodynamic properties of carbon at extreme conditions, build improved constitutive models and provide information for future designs for ICF at the NIF. In particular, we hope to resolve the discrepancy between current EOS and experimental data unveiled by the analysis of shock-timing experiments on the NIF and described in Ref. 9.

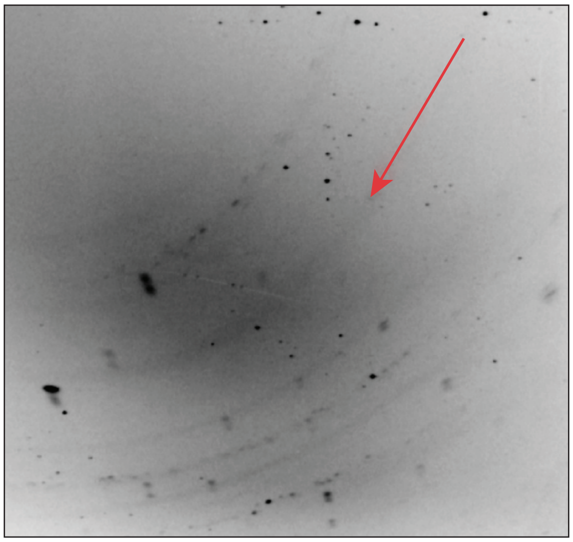
U2529JR

Figure 5
Example of raw powder x-ray diffraction image-plate (PXRDIP) data showing the x-ray diffraction pattern of diamond shock-compressed near 8 Mbar (red arrow), together with the calibration line.

Proton Radiography Measurements Using DT^{3}He–Filled Exploding Pushers as Proton and Deuteron Sources
Principal Investigator: B. B. Pollock
Co-investigators: G. Sutcliffe, C. Li, and J. D. Moody

MagHohlMultiPBL-19A is the first experiment in a campaign to probe hohlraum-relevant physics with protons and deuterons from a DT^{3}He-filled exploding-pusher source.

Figure 6 shows the general experimental geometry. The backlighter capsule location and drive were the same for all shots on the day, but the fill varied between DT^{3}He and D^{3}He. The capsules were driven by 39 beams of OMEGA, while the others were used for driving foil targets and for Thomson scattering. Two foil configurations were studied during the shot day. The first irradiated flat CH foils in both foil locations with six beams each, where protons (and deuterons if the capsule contained T) probed the electric and magnetic field structures at the target surface either through or tangential to the target face. In this configuration, 2ω Thomson scattering was performed at various locations relative to the surface of one of the target foils in order to measure electron density and temperature for comparison with simulations of the expanding surface plasma. The second configuration used Au foils in both locations, one flat and one curved; both foils were probed edge on with the protons and deuterons from the pusher. The maximum number of beams was reduced to either three or five, depending on the foil geometry, and the on-shot beam orientation was varied by dropping one or more beams from each shot. By changing the effective beam spacing, the resulting field structures are also affected and can be distinguished using the (up to) three charged particles emitted from the pusher. The proton data are still being processed, but initial estimates of the deuteron yield from the capsules containing T are approximately 3$\times$ less than initial estimates based on scaling from prior experiments. This discrepancy is being investigated further, and future experiments will attempt to drive the capsules with more energy to achieve higher yields.

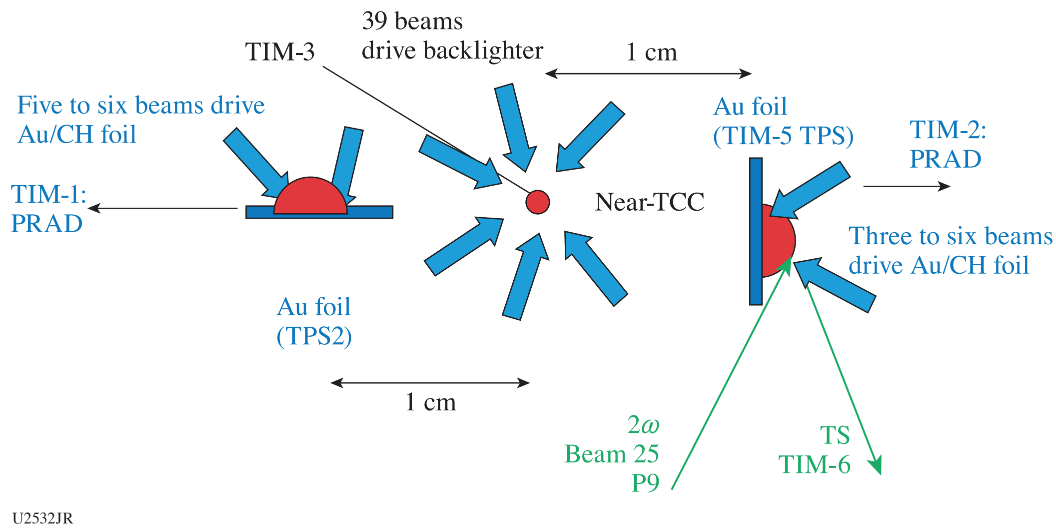

Figure 6
Experimental configuration for MagHohlMultiPBL-19A. Two foils are placed ~1 cm away from an exploding-pusher capsule target positioned near target chamber center (TCC). The capsule is filled with either DT^{3}He or D^{3}He. When compressed, both capsule fills produce 3.0- and 14.7-MeV protons; with T present in the fill, 9.5-MeV deuterons are also produced. These particles probe the electric- and magnetic-field structures either across or through the foil targets depending on the foil orientation. Protons and deuterons are recorded on CR-39 detectors.

Characterization of Compressed MIFEDS Fields in Cylindrical Targets
Principal Investigator: B. B. Pollock
Co-investigators: J. R. Davies and J. Peebles (LLE); and J. D. Moody (LLNL)

BFieldAmp-19A and 19B were the first experiments in this campaign to attempt to characterize compressed magnetic fields in cylindrical geometries on OMEGA.

Figure 7 shows the general experimental geometry for BFieldAmp-19A and 19B. The target for both shot days was an empty plastic tube of ~600 μm diameter with a 30-μm-thick wall. The tube is irradiated around its waist to drive >10× convergence of the tube diameter. Provided the inner wall of the tube is sufficiently ionized from x rays produced by the laser–wall interaction

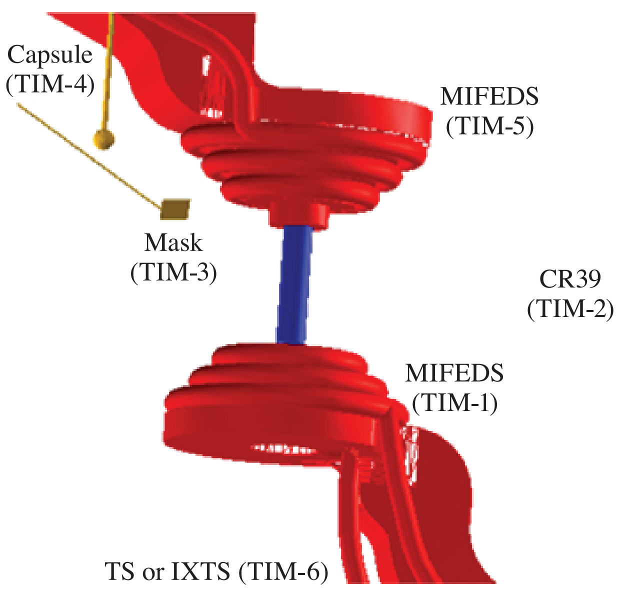

Figure 7
Experimental configuration for BFieldAmp experiments. A plastic tube (blue) is attached to one MIFEDS coil, while a second coil is inserted on the opposing side to allow for up to 30-T magnetic-field production at the center of the tube. The tube is irradiated with 40 beams around its waist to drive it radially inward from an initial diameter of ~600 μm to a final diameter of ~50 μm. Protons are produced from the implosion of a D^{3}He-filled capsule target, some of which are collected on a CR-39 detector on the opposite side of the tube from the capsule. The mask was present only in 19B and partially blocks the proton line of sight to the CR-39 on only one side of the tube. The optical Thomson-scattering collection system was used to measure plasma emission on 19A, while the imaging x-ray Thomson spectrometer (IXTS) system was used to measure x-ray emission on 19B.

on the exterior of the tube, the magnetic field should compress with the tube wall and result in an increased B-field strength proportional to the square of the tube's convergence ratio. The strength of the applied magneto-inertial fusion electrical discharge system (MIFEDS) magnetic field was varied from 5 to 30 T between the two shot days, and optical and x-ray emission measurements were taken to look for evidence of the magnetic-field compression. However, the proton data from these experiments are currently inconclusive about the compression of the initial magnetic field during the tube implosion, as are the spectroscopic measurements. Further analysis is underway, and future experiments will add a gas fill to the tube similar to that of the mini-MagLIF (magnetized liner inertial fusion) experiments of J. Davies *et al*.[10] The initial gas fill will provide the tube with material to push against, potentially reducing the convergence ratio, but in this configuration the gas has been shown to be able to be ionized by the x rays produced during the implosion and should therefore be more robust for entraining the initial magnetic field and compressing it as the tube implodes. Following a successful characterization of B-field compression, additional future work will use the high-field region at the compressed tube center as a platform for ultrahigh magnetic-field experiments.

Characterization of Laser-Driven Magnetic Fields
Principal Investigator: B. B. Pollock
Co-investigators: S. Fujioka, H. Morita, K. Law, and J. D. Moody

BFieldLoop-19A is a continuation of the laser-driven magnetic-field experimental campaign on OMEGA EP. The goals for 19A were to study current diffusion in the loop targets, as well as to examine the B-field dependence on target material choice for the loops.

Figure 8 shows data from four different shots on the day. Figure 8(a) is a radiograph of the loop target without driving the magnetic field. The loop target and the x-ray shield blocking the line of sight to the proton generation foil can be seen clearly in the image. The top of the target shows shadowed regions at the edges, corresponding to the location of the thin strap pieces that connect the front and back rectangular plate portions of the target, which are intended to restrict the ability of the current to diffuse away from the target edges. This configuration also produces a magnetic reconnection geometry between the straps, which may be investigated further in future experiments.

Figure 8(b) shows the result of driving a Au target with 0.5 TW of laser power for 3 ns, consistent with previous experimental configurations with complete loop sections at the target top. The lateral width of the shadowed region outside the outline cor-

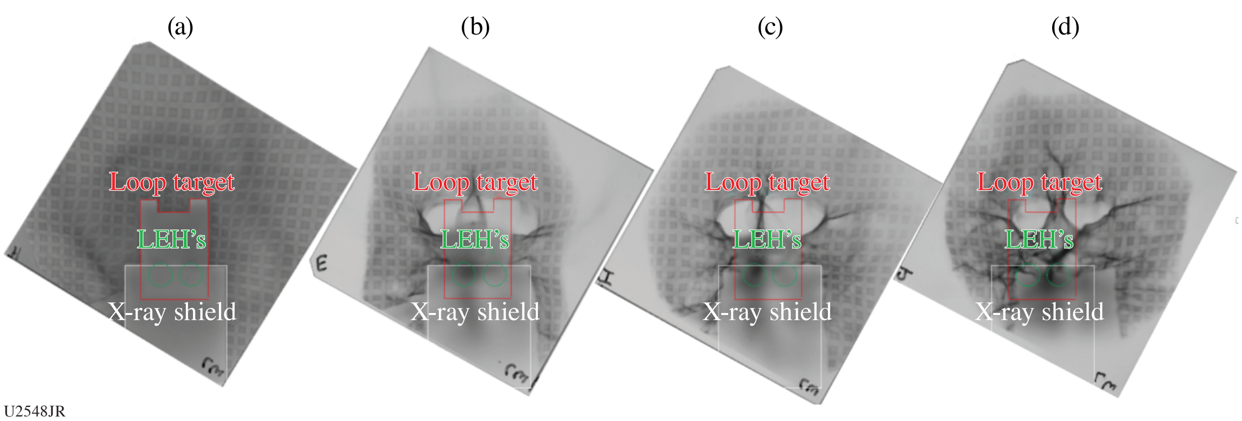

Figure 8
Proton radiography images for (a) undriven Au, (b) driven Au, (c) driven Cu, and (d) driven Al targets. The targets are foils folded to produce parallel rectangular plate sections that are 1.1 mm wide and 1.5 mm tall, with 300-μm-wide, 250-μm-radius straps at the edges connecting the plates (which are separated by 500 μm). The B field is produced by irradiating the target interior through one of the laser entrance holes (LEH's, typically the left side in these images), which generates a voltage difference between the plates, driving a current through the straps, resulting in a magnetic field around the top portion of the target. The x-ray shield blocks the line of sight from the LEH's back to a 10-μm-thick Au foil, which is irradiated by the 1-ps backlighter pulse on OMEGA EP at 200 J to produce the probing protons via the TNSA (target normal sheath acceleration) mechanism. A Cu mesh between the TNSA foil and the B-field target produces the grid structure in the images.

responding to the undriven target location is correlated with the strength of the magnetic field being produced around the straps, but there is also significant additional structure developing on the interior part of the target between the straps. Changing the target material to Cu shows an enhancement in this structure, as well as enhanced caustic features at the edges of the proton shadows around the straps. Reducing the target Z even further by using an Al target shows more structure still compared to the Cu and Au targets. These additional materials were initially chosen to study the effect of different conductivities and specific heats on current diffusion processes; the enhanced structures around the target location need further analysis to determine the full impact of target material choice on the current and B-field generation processes. These data are still being analyzed, but future experiments will measure the B-field structure in the non-Au targets at earlier evolution times as well as after the end of the pulse (as has been done previously with Au).

Experiments to Address Laser Transport in Magnetized Plasmas
Principal Investigator: D. Mariscal
Co-investigators: G. E. Kemp, E. Marley, and K. Tummel

Simulations using *HYDRA* with magnetohydrodynamic (MHD) packages predict enhanced laser propagation and plasma temperatures when magnetic fields are imposed along the laser axis, as seen in Fig. 9. These experiments explore parameters that produce magnetized plasmas (electrons) where these effects can be examined and used to determine which MHD terms are important for reproducing results in *HYDRA*.

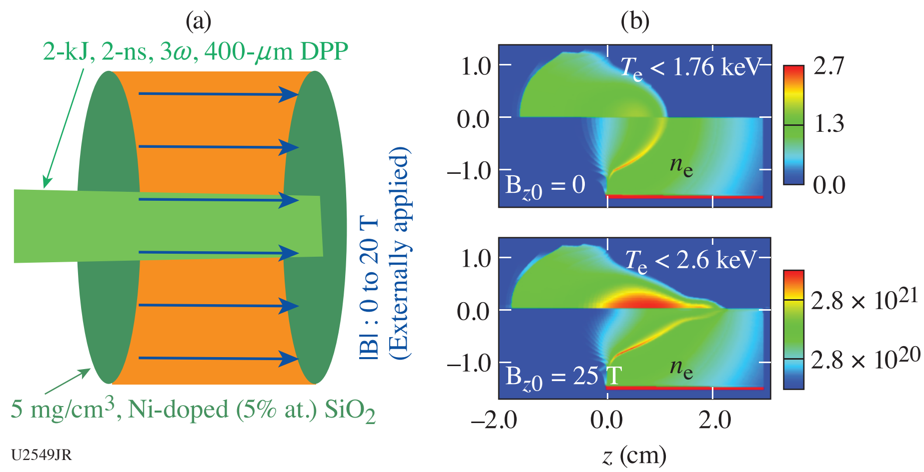

Figure 9
(a) Experiment and simulation setup in *HYDRA* showing orientation of axial B field along laser axis, cylindrical foam targets, and laser parameters. (b) Results from 2-D *HYDRA* calculations (K. Tummel) showing significant differences in both electron density and temperature profiles at 1.5 ns into the laser pulse.

Targets in these experiments were 3-mm-diam, 3-mm-long, 5-mg/cm^3 SiO_2 foams [see Fig. 9(a)] that were doped with Ni at ~5% atomic fraction in order to perform spectral measurements of the plasma temperature. These foams were mounted within MIFEDS coils with a quasi-Helmholtz geometry to provide a nearly uniform spatial profile magnetic field up to ~20 T [see Fig. 10(a)]. The targets were then driven by a single UV beam on OMEGA EP with ~2 kJ of laser energy in a 2-ns super-Gaussian pulse. Two geometries were employed such that either Beam 1 or Beam 4 was used to drive the targets, with each beam using a 750-μm or 400-μm distributed phase plate (DPP) providing ~2×10^{14} or ~1×10^{15} W/cm^2 laser intensity. With these parameters, the plasma density is $\sim 0.2\, n_e / n_c$ with temperatures of ~2 keV and as seen in Fig. 10(b), allows one to explore plasma Hall parameters up to ~1. The multipurpose spectrometer (MSPEC) was used to acquire spatially and temporally resolved x-ray data along the laser axis [see Fig. 10(c)], while an x-ray framing camera (XRFC) was used to image the heat-front propagation [Fig. 10(d)].

Over two shot days, 17 target shots were completed, resulting in both a successful platform demonstration and a data set scanning two intensities and four B-field values (0, 5, 10, and 19 T). Preliminary analysis seems to indicate a dip in propagation velocity in

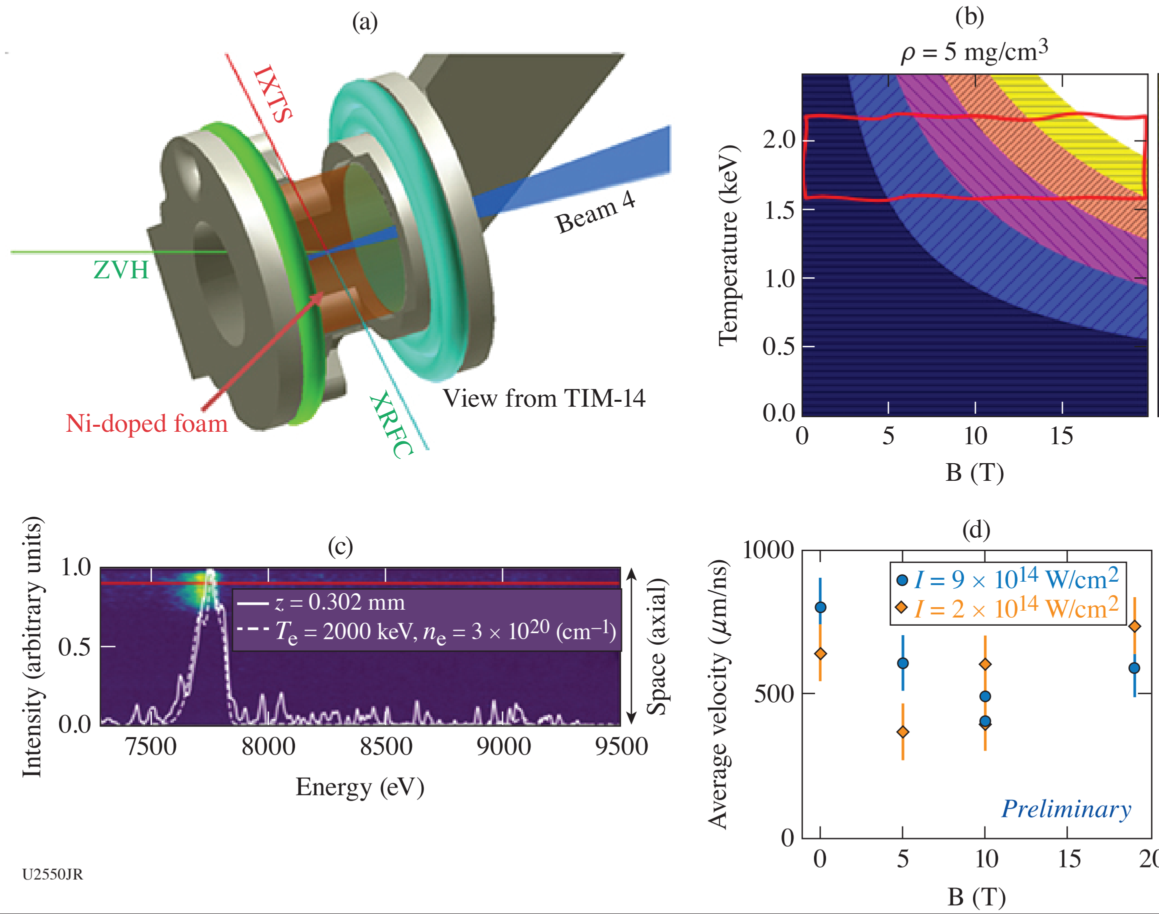

Figure 10
(a) Experimental setup showing MIFEDS coils and diagnostic locations. (b) The red box shows $\omega_{ce}\tau_{ei}$ space for the present experimental parameters at a fixed density. (c) Example MSPEC data, lineout, and corresponding fit. (d) Experimentally measured velocities showing a slowing of laser heat front near 5 to 10 T.

the neighborhood of 5 to 10 T. *HYDRA* simulations are underway to compare against this data set that should provide important insight regarding the importance of B fields in hydrodynamic calculations of laser-driven experiments at ICF-relevant conditions.

Experiment Study of Laser Entrance Hole Dynamics
Principal Investigator: J. Ralph
Co-investigators: M. Tabak, W. Farmer, O. L. Landen, and P. Amendt

These experiments tested several designs of the hohlraum LEH for use in advanced next-generation hohlraums. In total, 14 shots were performed to compare the LEH closure, hohlraum drive, and backscatter when using a variety of LEH types. The 1-mm-diam hohlraums were aligned to the H4–H17 axis; the surrounding six beams at 21.5° were focused at the 400- or 500-μm-diam LEH and incident on a 25-mm-thick Au plate located at about the middle of the hohlraum. The laser pulse used on all experiments is the 2-kJ pulse shown in Fig. 11(b). The x-ray framing camera timing (blue arrows) is shown relative to the laser pulse. We tested four types of LEH's: a simple opening; a 0.5-μm polyimide window; a CH-lined Au plate with a polyimide window; and, finally, a 100-μm-thick Au foam with a polyimide window.

All experiments used the same laser pulse. The mains results are summarized in Fig. 12. Here we see the 400-μm x-ray framing camera data from ten-inch manipulator TIM-3, looking in through the LEH, and TIM-2, looking at the hohlraum emission. The LEH-side framing camera measures the LEH closure as a function of time as shown in Fig. 12. We find the CH liner maintains the complete opening of 400 μm throughout the pulse. The TIM-2 framing-camera data shown in Fig. 12 provides a measure of the peak hohlraum emission using a 2° Ge mirror combined with a 1-μm Zn filter. From this data, the Au foam seems erratic, low at early time and high later in the pulse. The remaining LEH designs show an overall decline with time. Neglecting the Au foam data, it appears that during the middle of the pulse, the CH-lined LEH results in about 25% more emission. These results will provide information for future experiments and designs on the NIF.

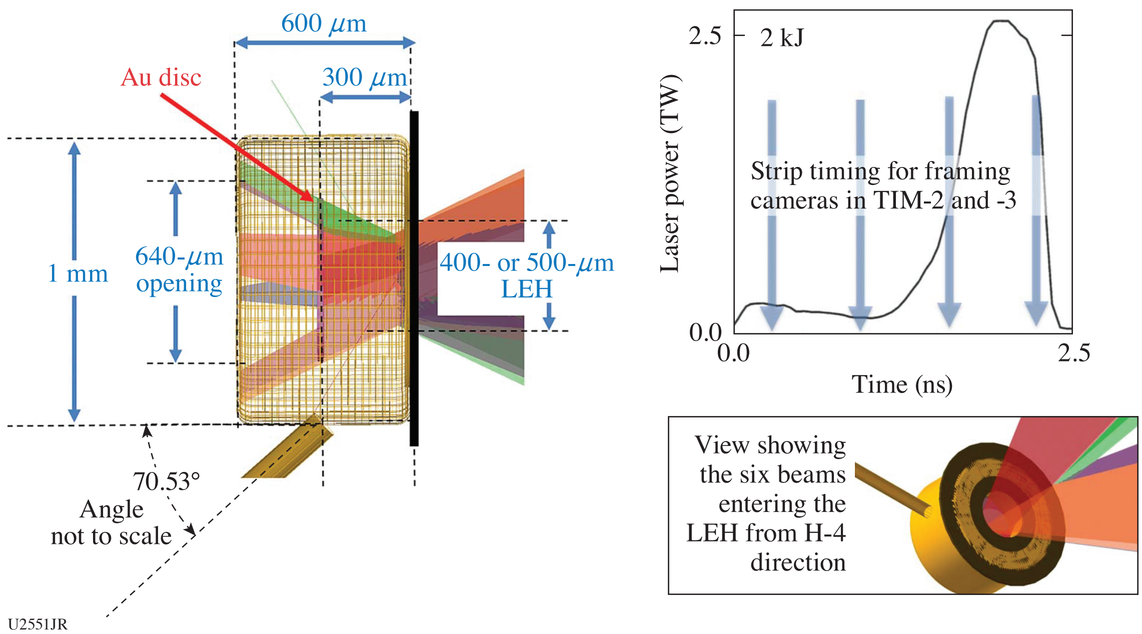

Figure 11
Target and experimental configuration.

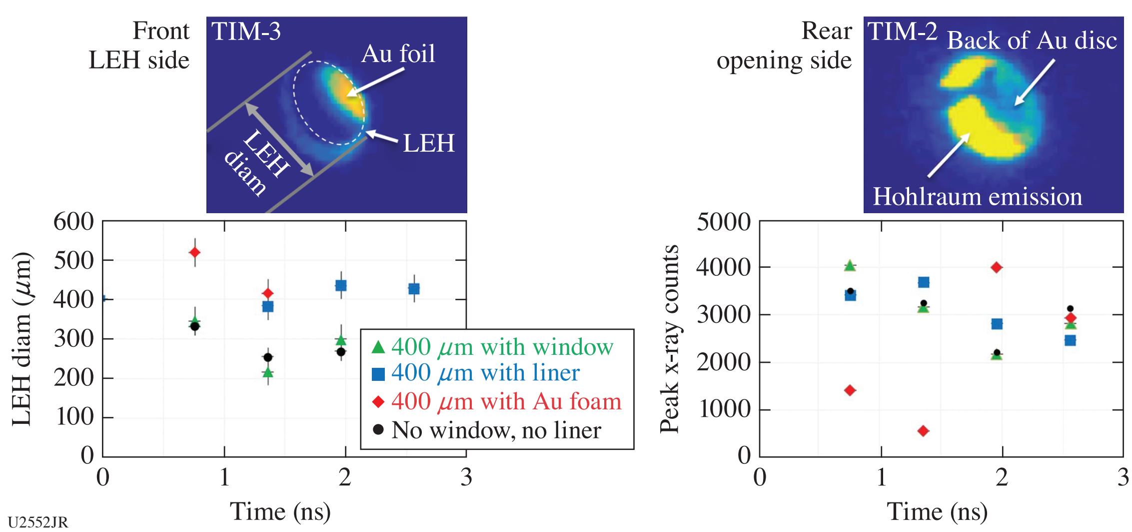

Figure 12
X-ray framing camera data.

Assessing Heat Transport in the Transition Between Local and Nonlocal Regimes
Principal Investigator: G. F. Swadling
Co-investigators: W. Farmer, M. Sherlock, M. Rosen, and B. B. Pollock (LLNL); D. H. Edgell (LLE); and C. Bruulsema and W. Rozmus (UA)

In the BeSphere-19A Campaign, we performed experiments that heated beryllium-coated spheres in a direct-drive geometry. The experiments were diagnosed using the OMEGA Thomson-scattering system (TSS), scatter calorimeters, and the Dante x-ray spectrometer. The aim of these experiments was to make quantitative measurements of the parameters of the blow-off plasma produced from these spherical targets. Seven target shots were completed in the half-day.

The data from these experiments are currently being used to benchmark heat-transport models. Using beryllium as the target material eliminates complications introduced by the high radiative losses and complex atomic physics of gold. To further simplify comparisons between experiment and simulation, the targets were heated at comparatively low intensities of 1 to 2.5 × 10^{14} W/cm^2; at these intensities, coupling the laser to the target was shown to be better than 90%.

The Thomson-scattering diagnostic measured the time-resolved spectrum of light scattered by fluctuations in n_e with wave vectors $\vec{k}$ tangential to the surface of the sphere. The size of the scattering volume, defined by the overlap of the probe beam and collection cone, was ~(50 μm)^3. Measurements were made at locations 200, 300, and 400 μm from the sphere surface. The diagnostic recorded scattering from both high-frequency electron plasma wave fluctuations (EPW, T_e, n_e) and low-frequency ion-acoustic wave fluctuations (IAW, T_e, T_i, v_{flow}). Examples of the data recorded are shown in Fig. 13. Fitting these measured spectra results in quantitative measurements of the plasma parameters, which may be compared with the results of numerical modeling. As an example, the T_e and T_i profiles measured in the experiment are compared with those calculated in a *LASNEX* run in Fig. 13, illustrating that good agreement was achieved.

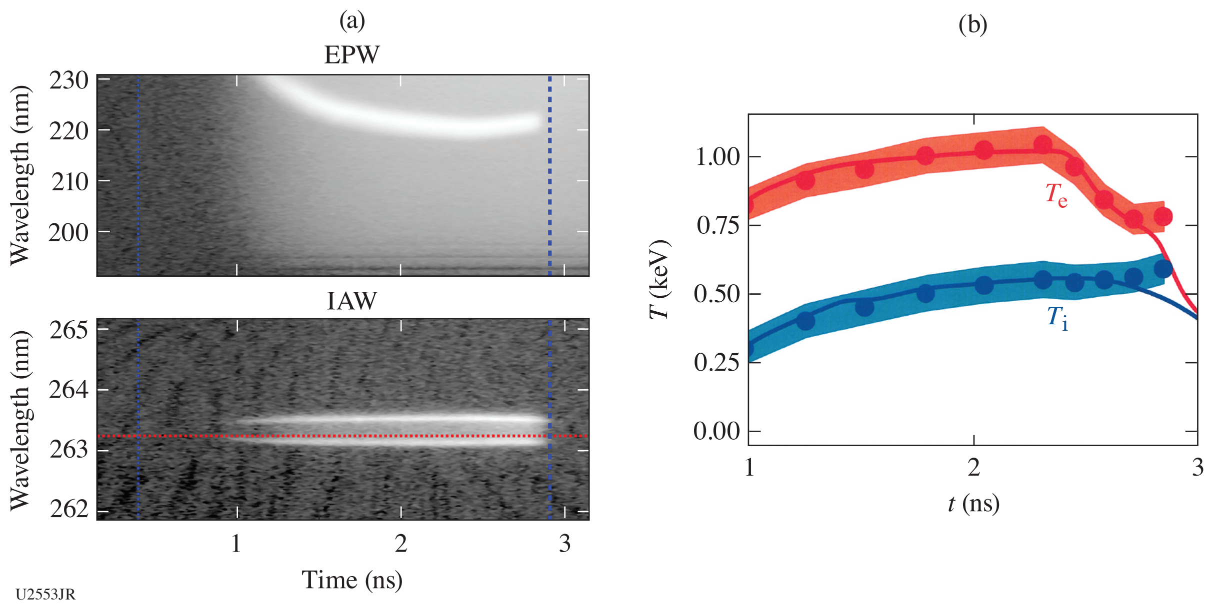

Figure 13
(a) Raw IAW and EPW Thomson-scattering spectra. (b) Example of a comparison between plasmas parameters measured by fitting the Thomson data and those calculated in a *LASNEX* simulation of the experiment. The circles are measurements, the shaded band indicates experimental uncertainly, and the solid lines show the *LASNEX* values.

Generation of TNSA Short-Pulse Laser-Accelerated Deuterons with up to 30-ps Pulse Length
Principal Investigator: J. Park (UCSD)
Co-investigators: J. Kim and F. N. Beg (UCSD); and T. Ma, D. Mariscal, G. Cochran,* and A. Zylstra (LLNL)
Graduate student: R. Simpson (MIT)
*Postdoc

This series of shots investigated the generation of proton and deuteron beams via short-pulse laser acceleration using the TNSA mechanism in the multi-ps regime. CD foils of 35-μm thickness were illuminated by OMEGA EP short-pulse beams with a varying pulse length (1 to 30 ps) and intensity (10^{17} to 10^{18} W/cm^2), relevant to NIF ARC (Advanced Radiographic Capability) laser conditions. Over the course of the day, the two OMEGA EP short-pulse beams were alternated in single-beam shots: Beam 1 delivered between 100 J and 300 J of energy on targets over 1- or 3-ps pulse length, while Beam 2 delivered between 625 J and 1250 J of energy over 10 ps or 30 ps. Both beams were defocused, ~45 μm R/80, to achieve the desired laser intensity. Several target shots utilized a novel configuration of combining both beams to provide a temporally shaped pulse to test proton and deuteron generation.[11] On this shot, the two beams were spatially overlapped on the target, but Beam 1 (3 ps) arrived prior to Beam 2 (30 ps) by ~45 ps. Three diagnostics were used to measure proton, deuteron, and electron spectra with varying laser conditions: radiochromic film (RCF) along the target rear normal, a Thomson parabola ion energy (TPIE) analyzer, and an electron spectrometer (E-spec) at 45° from the target rear normal (Fig. 14).

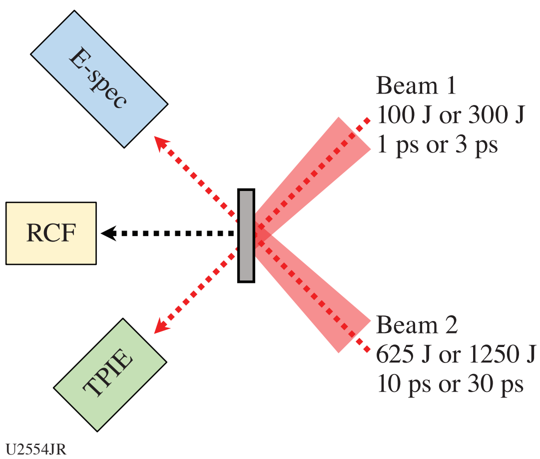

Figure 14
Top-down view of the experimental setup.

It was observed (Fig. 15) that there is a strong scaling of the ion flux and maximum ion energy with laser energy when a single beam is utilized; a 3-ps-long pulse with 100 J generated protons up to 3.6 MeV but no observable deuterons, while a 30-ps-long pulse with 625 J generated protons up to 5.1 MeV and deuterons up to 1.8 MeV. When both beams were simultaneously used, the maximum energy increased to 6.8 MeV and 4.9 MeV for protons and deuterons, respectively. The electron flux was also significantly increased by up to 7× when comparing single-beam to dual-beam configurations. The increase in the maximum ion energy due to this increased electron flux or the electron temperature is still under investigation.

Increasing Laser-Accelerated Particle Energies with "Shaped" Short Pulses
Principal Investigator: D. Mariscal
Co-investigators: T. Ma and G. Cochran* (LLNL); and J. Park* and J. Kim* (UCSD)
*Postdoc

Newer kJ-class, short-pulse (ps) lasers such as the NIF's ARC laser have recently been shown to be able to accelerate protons to energies that far exceed conventional scalings. While these results are encouraging, the proton energies necessary for probing indirectly driven ICF experiments are 2× higher than currently achievable with ARC. A new concept inspired by a unique ARC capability—the ability to deliver multiple short-pulse beams to the same location with specified delays—was tested on OMEGA EP by delivering both short-pulse beams to a single target in order to create pseudo-shaped short laser pulses.

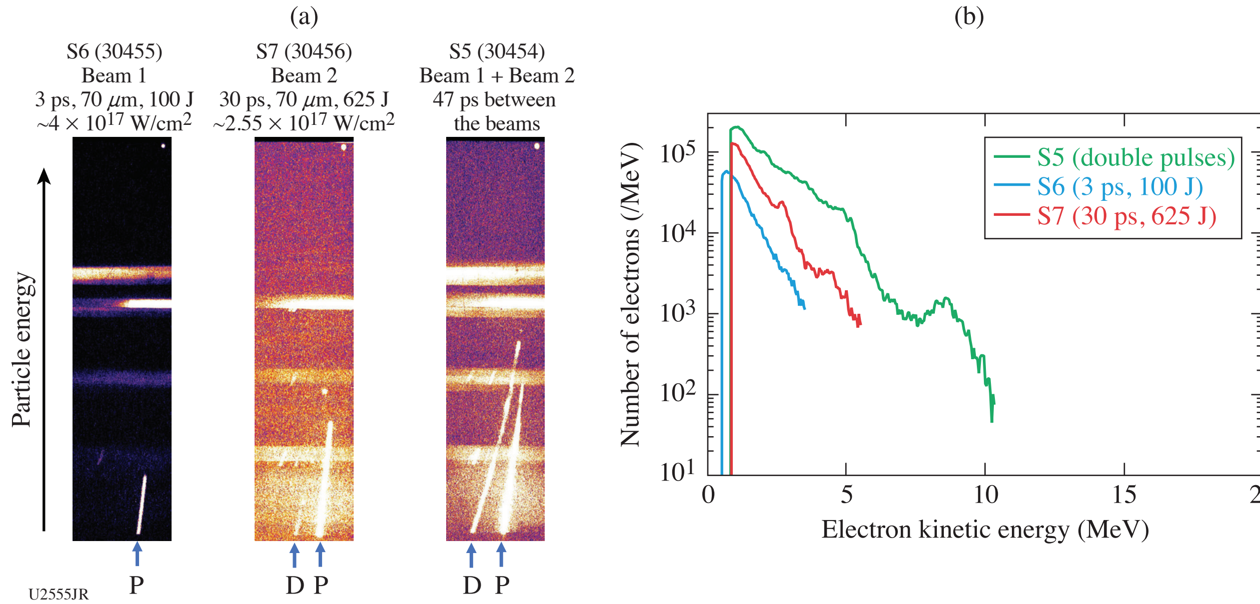

Figure 15
(a) Raw data from TPIE and (b) electron spectra from CD targets with three different laser configurations.

The experimental geometry is shown in Fig. 16. Both short-pulse beams were defocused to $R_{80} \sim 45$ μm in order to simulate ARC-like laser conditions. One beam delivered 550 J at 4 ps, while the trailing beam delivered 1.6 kJ at 30 ps. Simple flat Cu foils (1 mm diam × 35 μm thick) were used as targets. The choice of Cu enabled the use of the spherical crystal imager (SCI) instrument to monitor spatial overlap of the two beams on target, while the ultrafast x-ray streak (UFXRS) camera and time-resolved channel of the high-resolution spectrometer (HRS) monitored the relative timing of the beams on target. Particle diagnostics including RCF and the electron positron proton spectrometer (EPPS) were used to monitor the particle characteristics for each shot. Particle spectra were recorded from single-beam shots before combining the beams and varying the relative timing between the two throughout the day.

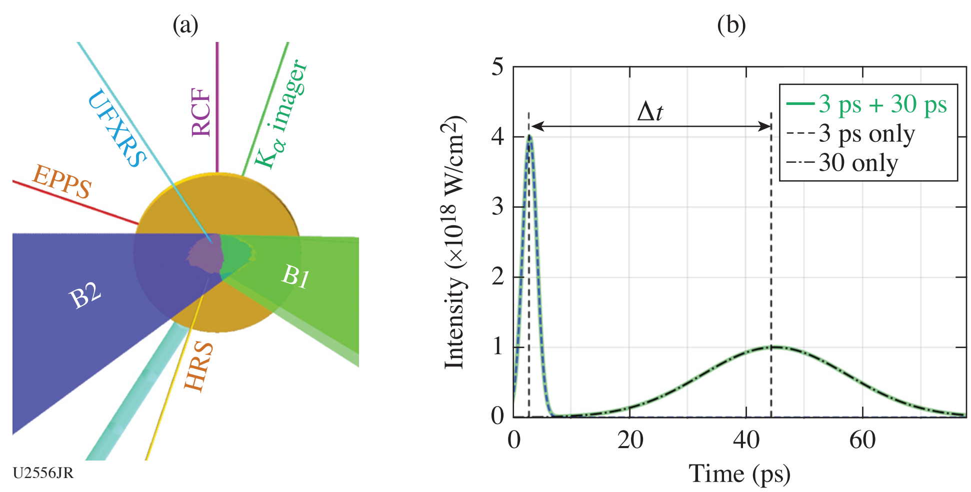

Figure 16
(a) Experimental configuration showing the two short-pulse beams incident on the foil target and the location of the diagnostics; and (b) an example of the pulse shapes and definition of Δt for Fig. 17.

A successful day with nine data shots was completed (four single beam + five combined beam). A preliminary look at the data (Fig. 17) indicates that electron temperatures and yields were significantly increased when pulse combinations were used, with a factor-of-2+ increase in total conversion efficiency into hot (>1-MeV) electrons, 50% increase in electron temperature, and a corresponding 50% increase in maximum proton energy. These data suggest that the use of shaped short pulses could increase the energy and efficiency of MeV particle sources driven by the NIF's ARC by manipulating time-dependent particle acceleration physics at the picosecond level. These novel results stimulated follow-up experiments now scheduled in FY20.

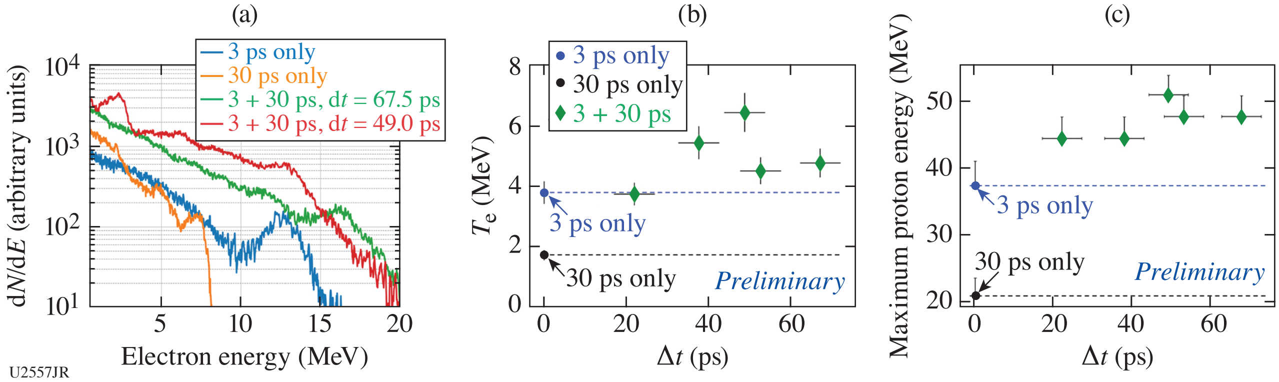

Figure 17
(a) Several electron spectra from the EPPS spectrometer and analysis showing (b) the exponential temperature fits to the data and (c) the maximum proton energy from RCF stacks for each case. All data are plotted versus the delay between the two beams.

Development of Improved Backlighters Using In-Situ *Plasma Reflectors*

Principal Investigator: R. Tommasini
Co-investigators: J. Park, L. Divol, and A. Kemp

The SmallSpotBL-EP-19 Campaign continued the development and testing of novel small-source x-ray backlighters that started with the prior campaign, SmallSpotBL-EP-17. The concept is to use *in-situ* plasma mirrors to enhance the laser energy coupling on microwire backlighters that can be used as point sources in high-energy x-ray radiography and at the same time increase the tolerance to laser pointing jitter.

In this campaign we introduced an improvement of the plasma mirror geometry by using 25-μm-diam Au microwires at the vertex of parabolic-like CH profiles, for brevity U-shaped PM (Fig. 18).

The 30-ps-long, 1-kJ energy pulses from the OMEGA EP sidelighter beam were pointed at the vertex of the plasma mirror profile. The x-ray yield and source size were measured along the line of sight aligned parallel with the gold wire, by radiographing a tantalum step wedge and a calibrated tungsten sphere, 200 μm in diameter.

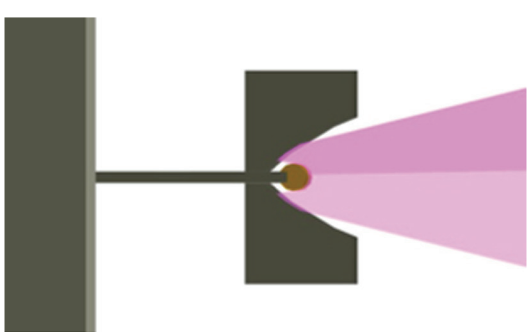

Figure 18
End-on view of 25-μm-diam Au wire in a U-shaped plasma mirror, illuminated by the OMEGA EP sidelighter beam.

We also performed shots with the original V-shaped CH profiles (V-shaped PM) and with bare Au wires. The results have confirmed a 2× to 3× increase in conversion efficiency when using the V-shaped plasma mirror configuration as compared to bare wires, and a 4× to 5× increase when using the U-shaped plasma mirror configuration. We also reported reduced statistical variation in x-ray yield between shots. The backlighter source size when using plasma mirrors has measured similar or smaller in size with respect to bare microwires and always very close to the wire diameter.

These novel backlighters are ideal for hard x-ray radiography of ICF implosions and make it possible to reduce the backlighter size in order to record radiographs with higher spatial resolution while maintaining sufficient signal-to-noise ratio. They have been used to record Compton radiographs of the imploding fuel on two layered THD shots on the NIF.

High-Energy-Density Experiments

1. Material Equation of State and Strength Measured Using Diffraction

X-Ray Diffraction of Shock-Ramped Platinum

Principal Investigators: A. E. Lazicki (LLNL) and M. Ginnane (LLE)
Co-investigators: R. Kraus, J. H. Eggert, M. Marshall, and D. E. Fratanduono (LLNL); D. N. Polsin, X. Gong, T. R. Boehly, J. R. Rygg, and G. W. Collins (LLE); and J.-P. Davis, C. McCoy, C. Seagle, and S. Root (SNL)

This campaign seeks to determine the structure of platinum (Pt) at high temperatures and pressures. Platinum is of interest because it is often used as a pressure calibration standard in diamond anvil cell experiments due to its low reactivity and wide pressure–temperature stability. Shock-ramp experiments on Sandia's Z machine have suggested evidence of a phase transition occurring at ~150 GPa. The inverse Z method applied to Pt by L. Burakovsky[12] suggests a solid–solid phase transition in a similar pressure region. The goal of this experiment was to use x-ray diffraction (XRD) to study the crystal structure at the pressure regime where a new phase is suggested. A series of measurements was carried out using the powder x-ray diffraction image-plate (PXRDIP) platform on OMEGA EP. The target package consisted of a Be ablator, a 25-μm Al foil, a 7-μm Pt foil sample, and a 130-μm LiF window. The thickness of the Be ablator was varied between shots in order to reach different shock pressures (50 to 200 GPa). Two 10-ns UV beams were combined to create a 20-ns drive that shocked the sample and then ramp compressed to various pressures, up to ~500 GPa. A Ge backlighter foil was driven to create a 1-ns flux of 10.25-keV x rays that were diffracted by the target package and collected on the image plates shown in Fig. 19. The ASBO telescope was focused at the sample/LiF interface and used to infer a pressure history in the Pt.

Six of the seven shots had either three or four solid diffraction lines, consistent with the face-centered cubic (fcc) phase. In the remaining shot, liquid diffraction is believed to have been observed, but blanking in ASBO means the exact pressure is unable to be determined using the usual method. Initial hydrodynamic simulations suggest the Pt was shocked to >800 GPa. This last shot will provide information for an upcoming shot day to determine where Pt melts on the Hugoniot.

Laue Diffraction from Ta Using a Cu Foil Backlighter

Principal Investigator: A. Krygier
Co-investigators: C. E. Wehrenberg and H.-S. Park

The TextureDiff-19A experiment investigated deformation in [100] and [110] single-crystal tantalum at high pressure. Twinning has been found to play an important role in deformation under some conditions in tantalum, and this experiment was motivated to investigate this effect in single-crystal samples. Additionally, previous measurements of diffraction from single-crystal samples have not been able to constrain the *in-situ* density due to the nature of the technique. This experiment developed a new technique to simultaneously measure density and strain anisotropy in single-crystal samples (Fig. 20).

A shock wave was driven into the samples using direct laser ablation. The strength of the material produces strain anisotropy, where the sample is more compressed in the loading direction than the transverse directions. We probed this with white-light x-ray diffraction. Previous measurements of this sort used a capsule implosion to produce the smooth, high-flux, short-duration x-ray

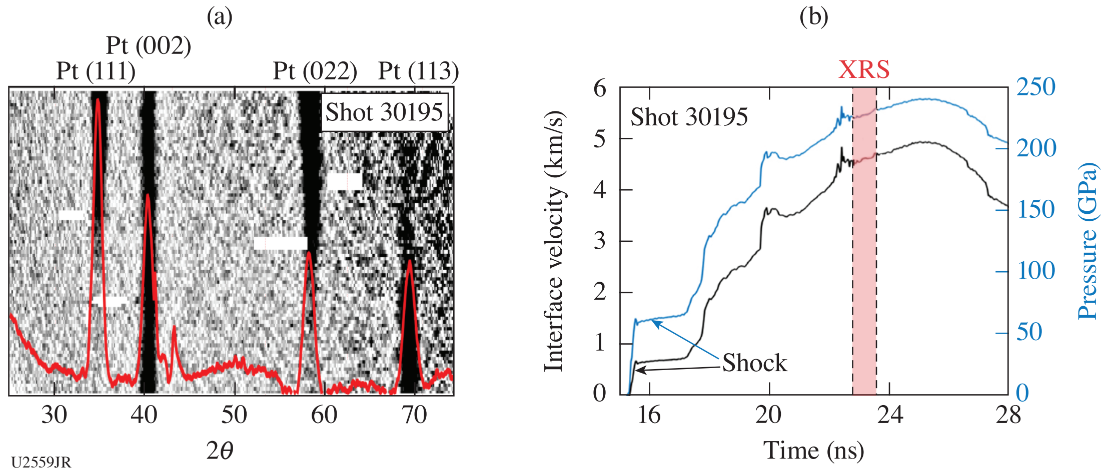

Figure 19
(a) Example diffraction data showing four lines generated by solid Pt in the fcc phase. (b) The sample particle velocity, inferred pressure profile, and timing of the x-ray source (XRS) obtained from VISAR.

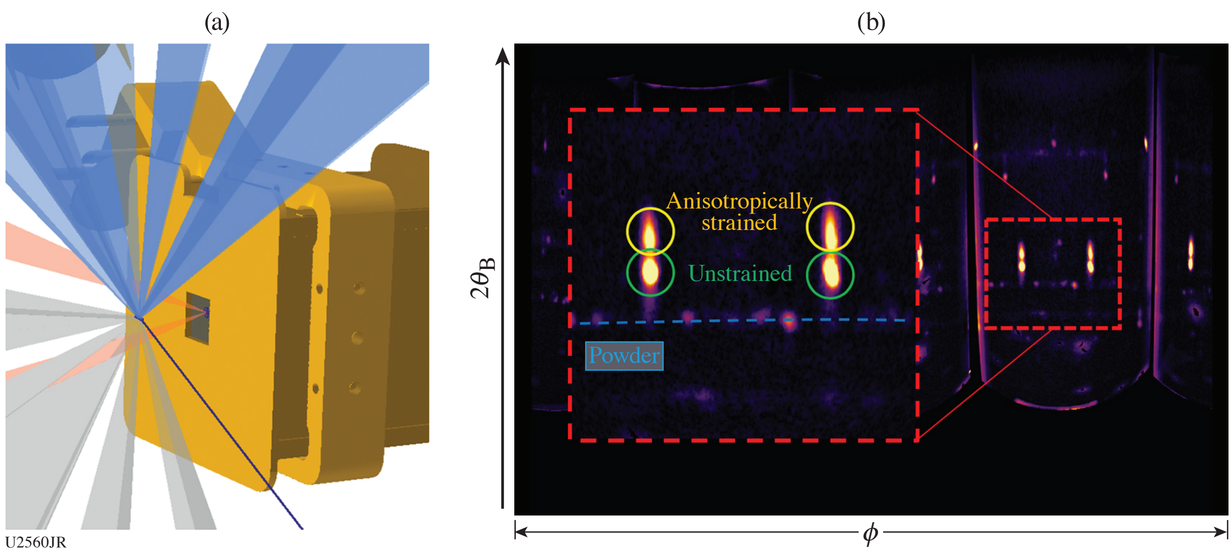

Figure 20
(a) One to two beams drive a shock wave into the Ta sample package. Nineteen beams heat a Cu or Au–Cu foil to produce white-light + He$_\alpha$ x-ray pulse. (b) Example data from [100] Ta. In the inset, green circles show the undriven Laue reflections; yellow circles show the anisotropically strained reflection that arises due to strength at high pressure. The dashed blue line shows powder diffraction from the monochromatic Cu He$_\alpha$.

pulse. We additionally probed the sample velocity using the ASBO diagnostic. We tested using a foil backlighter for this purpose, based on observation of x-ray flux enhancement made by the Extended X-Ray Absorption Fine Structure (EXAFS) Campaign. By using a copper foil backlighter, the x-ray spectrum has both a broad white-light feature useful for measuring strain anisotropy with Laue diffraction, as well as quasi-monochromatic He$_\alpha$ emission that is used to measure density with powder diffraction from polycrystalline samples and geometrically allowed single-crystal reflections. We also tested Au–Cu foils to compare bremsstrahlung emission but found this dramatically increased unwanted probe heating to the sample. This capability has the added bonus of enabling the use of PXRDIP instead of BBXRD, which improves the quality of the diffraction due to the geometry.

Probing the High-Pressure Crystal Structure of Lithium Fluoride
Principal Investigator: M. Gorman
Co-investigators: R. Smith and C. E. Wehrenberg

These experiments explored the high-pressure phase diagram of lithium fluoride. A structural transformation from the B1 phase to the B2 phase has been predicted.[13] Observing this transition may explain why nonlinear corrections to the refractive index of LiF are required in ramp-compression experiments on the NIF.[14] The target design is shown in Fig. 21(a). A 50-μm polycrystalline LiF sample was sandwiched between a 40-μm diamond ablator and a 100-μm MgO window. The OMEGA VISAR (ASBO) measures the LiF/MgO particle velocity from which the sample pressure as a function of time can be determined[15] as shown in Fig. 21(b). In these experiments we combine nanosecond x-ray diffraction[15] and ramp compression to dynamically compress and determine the crystal structure of LiF to peak pressures up to 600 GPa. Using the OMEGA PXRDIP diagnostic,[15] the compressed LiF sample is probed with a 2-ns He$_\alpha$ x-ray source to determine crystal structure at a well-defined sample pressure (VISAR). An example of the quality of the data obtained is shown in Fig. 21(c). Here we obtain information on the high-pressure B1 phase of LiF. Also observed are peaks from the ambient pressure Ta pinhole, which serve to calibrate diffraction angle. We find that LiF remains in the B1 phase up to at least 600 GPa along a quasi isentrope.

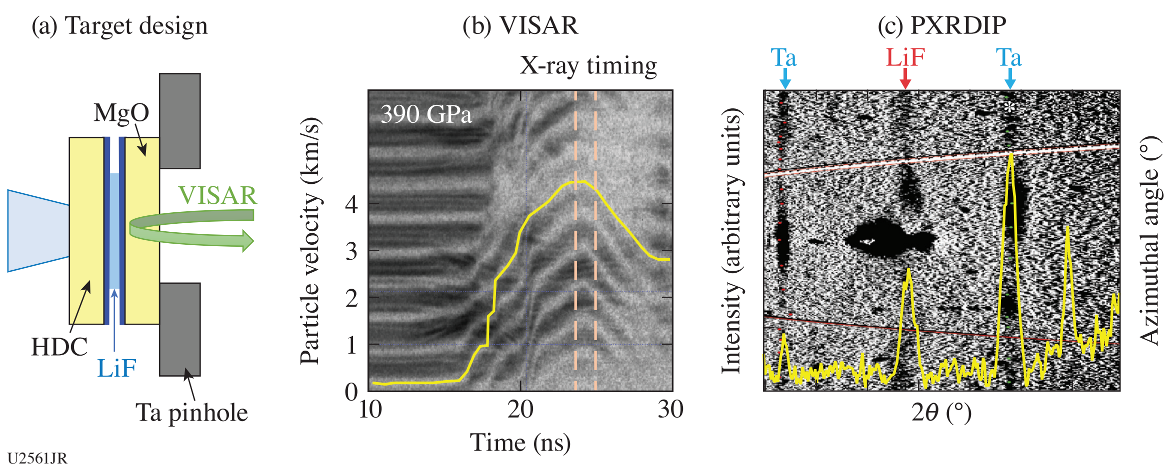

Figure 21
(a) Typical target design with a 40-μm diamond ablator, a 50-μm polycrystalline LiF sample, and a 100-μm single-crystal MgO window. (b) Raw VISAR fringe data with analyzed velocity profile overlaid. (c) De-warped PXRDIP diffraction data with 1-D lineout overlaid. The profile shows diffraction from the B1 phase of LiF at 390 GPa.

Development of a Time-Resolved X-Ray Diffraction Platform on OMEGA EP
Principal Investigator: L. R. Benedetti
Co-investigators: F. Coppari (LLNL); and D. N. Polsin, J. R. Rygg, and C. Sorce (LLE)

Based on the work performed in 2018, in which we learned that there was substantial electromagnetic pulse upset caused by the proximity of the large PXRDIP box to the x-ray streak camera, we completely redesigned the OMEGA EP time-resolved diffraction test platform. In the new platform [Fig. 22(a)], we removed the PXRDIP box (and associated image plates) and replaced it with a baffle/shield that prevents light from the backlighter from directly hitting any diagnostic. We are now also testing an XRFC for imaged diffraction (in addition to the x-ray streak camera) because the XRFC may be better shielded than the x-ray streak camera. As with the x-ray streak camera, dedicated hardware is required to maneuver the XRFC to an appropriate location to collect diffraction.

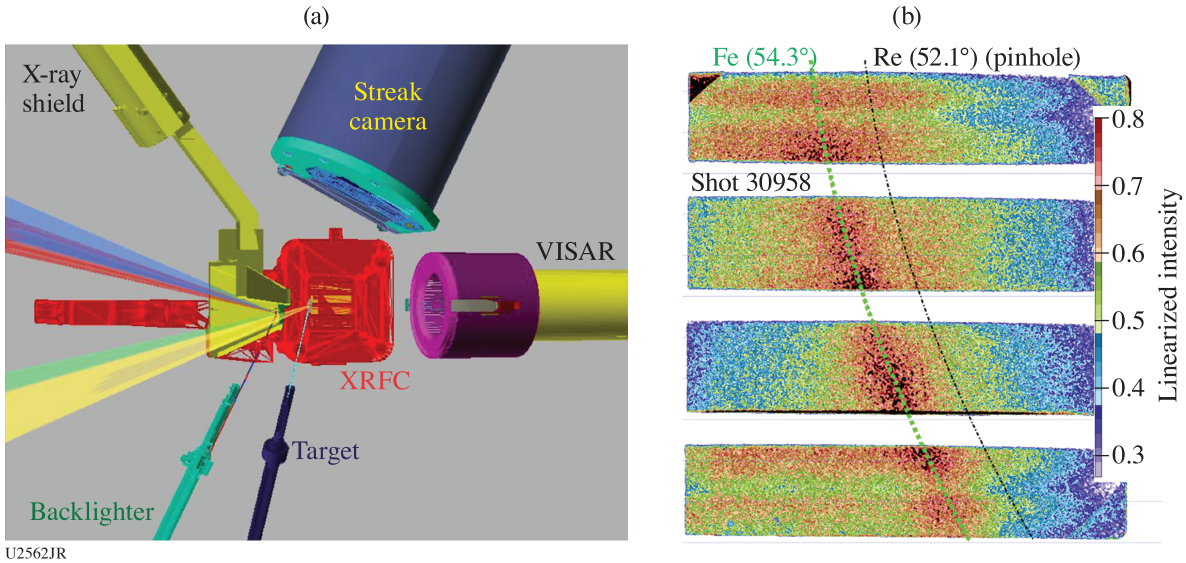

Figure 22
Imaged x-ray diffraction on OMEGA EP. (a) Updated experimental setup that maximizes distance between shielding elements and SSCA. (b) X-ray diffraction to XRFC of undriven Fe. Calculated diffraction is shown as an overlay.

We used this experimental setup on two shot days in FY19, during which we collected two diffraction patterns of undriven iron onto the XRFC [Fig. 22(b)]. Ongoing challenges are alignment accuracy, photometrics, and still-unexplained background signals along the streak camera's line of sight.

New Approach to Pressure Determination in Diffraction Experiments Using an* In-Situ *Pressure Standard
Principal Investigator: F. Coppari
Co-investigators: J. H. Eggert and R. Kraus (LLNL); and M. Vasquez (CalPoly, summer student at LLNL)

The goal of the *In-Situ* Pressure Campaign is to develop a new way to determine pressure in diffraction experiments based on the use of an *in-situ* pressure gauge. By measuring the diffraction signal of a standard material (whose pressure–volume equation of state is known) compressed together with the sample, one can determine the pressure upon ramp compression from the volume determined from the measured diffraction pattern.

Currently the pressure is determined by measuring the diamond free-surface velocity or particle velocity through a transparent window (such as LiF) using VISAR. This method is in some cases ambiguous (lack of reflectivity or shock formation) or relies on assumptions and equation-of-state models for the window materials. Cross-checking the VISAR measurement with *in-situ* pressure determination using the diffraction signal of a standard material will improve the diffraction platform by providing a complementary way of determining the pressure state within the sample, with great impact to the programmatic effort of determining structures and phase transitions at high pressure and temperature. In addition, combining pressure determination from VISAR and from the *in-situ* gauge can give us information about the temperature of the sample by measuring the calibrant thermal expansion.

We collected 12 successful shots in two half-days on the OMEGA laser, where we continued the work started in the previous FY, pushing it to higher pressure. The targets consisted of diamond ablators, Au/Ta or Pt/W coatings as *in-situ* pressure standards, and a diamond or LiF window [Fig. 23(a)]. We reached pressures as high as ~600 GPa and collected very good quality diffraction data (12 shots) in two half-days [Fig. 23(b)]. Simultaneous VISAR data were also collected. Data analysis is being finalized and comparison of the pressures obtained from VISAR and diffraction will provide information on the accuracy of the VISAR method as well as the existence of preheating. If successful, this platform will be implemented into a real diffraction experiment to be used as either a complementary or an alternative way to determine pressure and will also be developed on other experimental facilities such as NIF, XFEL, and synchrotrons.

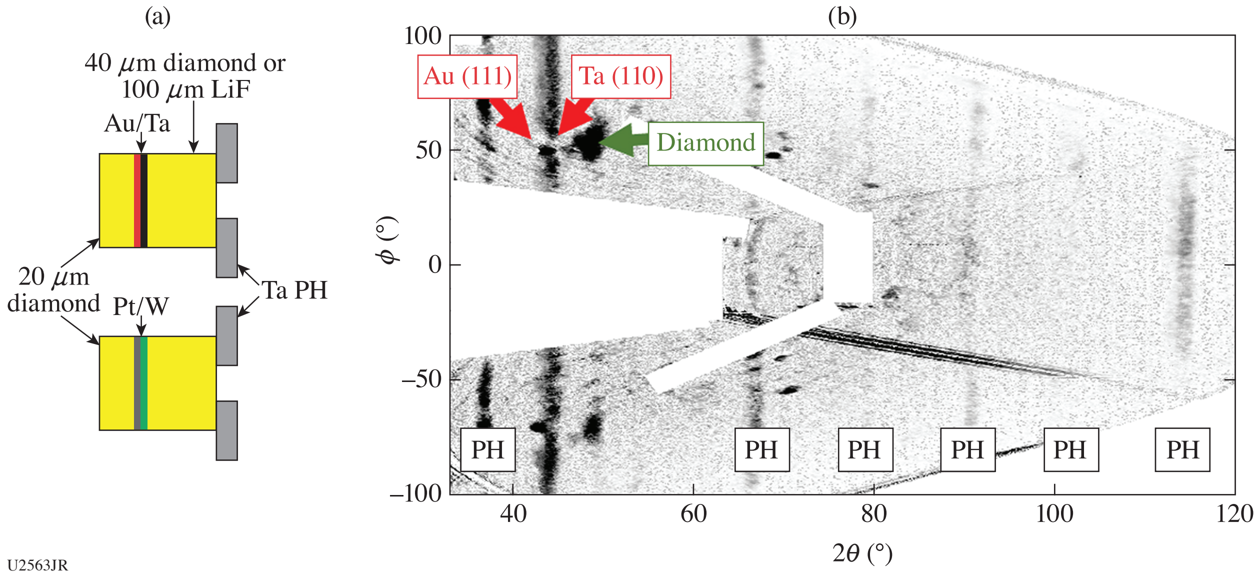

Figure 23
(a) Schematic of the target assembly. Diamond or LiF windows were coated with 1-μm-thick Au/Ta or Pt/W pairs used as pressure standards in the diffraction experiment. All targets had a 20-μm diamond ablator and were mounted on Ta pinholes. (b) Diffraction data collected in one of the experiments using Au/Ta as standards. At least one peak from compressed Au or Ta is visible, as well as lines from the Ta pinhole (PH) used to calibrate the diffraction geometry and single-crystal Laue spots due to the diamond. Cu He_{α} radiation (~8.4 keV) was used to obtain the diffraction data.

Development of the New Forward/Backward X-Ray Diffraction Diagnostic
Principal Investigator: A Krygier
Co-investigators: C. E. Wehrenberg, H.-S. Park, and J. H. Eggert (LLNL)

This experiment was the first effort at development of the new forward/backward x-ray diffraction diagnostic (Fig. 24). By using two monochromatic x-ray sources, we will be able to constrain the *in-situ* strain anisotropy induced by material strength in a polycrystalline sample. In this experiment we tested several design features: First, we measured the first reflection diffraction on OMEGA using a floating Fe microfoil with no pinhole. Second, we optimized the reflection x-ray cone shield, finding that a larger cone performed significantly better, with low background. Third, we tested a U-6 wt% Nb sample pinhole used in transmission

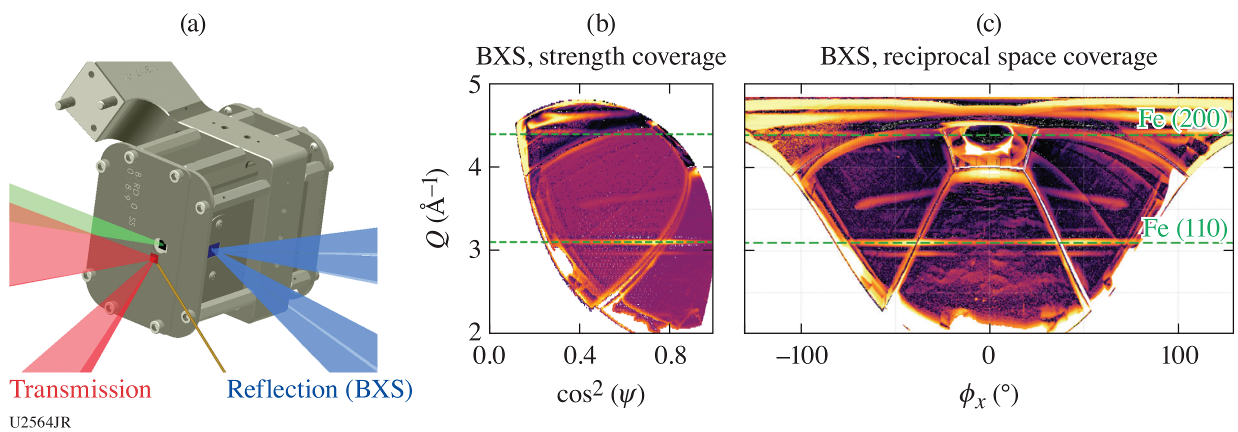

Figure 24
(a) Experimental setup. (b) Reflection diffraction from undriven Fe, displayed versus $\cos^2\psi$, the important parameter for strength; ψ is the angle between the diffracting plane and the applied stress. (c) The same data projected in reciprocal lattice–azimuthal coordinates. Extra reflections are from multiple emission lines from the Ti backlighter. An extraneous signal is also seen between the [110] and [200] Fe reflections.

diffraction on the NIF, finding that it produces unwanted x-ray diffraction in the reflection geometry. Finally, we confirmed high-quality diffraction in the transmission configuration with the extra features required for reflection diffraction (shield cone, etc.).

2. Material Equation of State Using Other Techniques

Equation-of-State Measurements Using Laser-Driven Mo Flyer-Plate Impacts
Principal Investigator: F. Coppari
Co-investigators: R. London, P. M. Celliers, M. Millot, A. Lazicki, and J. H. Eggert

The goal of the campaign is to develop a platform for absolute EOS measurements by laser-accelerated symmetric flyer-plate impacts.

The conceptual design is to use ramp compression to accelerate a molybdenum (Mo) flyer across a vacuum gap through indirect laser ablation and observe the flyer impact on a same-material sample, mounted side-by-side to a quartz window [Fig. 25(b)]. Velocity interferometry measurements with VISAR allow us to measure the flyer acceleration (U_{fs}) through the transparent quartz window, providing a measure of U_{p_impact} (for a symmetric impact: $U_{p\_impact} = 0.5 * U_{fs\_impact}$). The resulting shock state in the Mo sample is determined via transit time by measuring the time difference between the impact (t_{Mo_impact}) and the shock breakout (t_{Mo_BO}). The shock velocity U_s is then determined from $U_s = T_{Mo} / (t_{Mo\_BO} - t_{Mo\_impact})$, where T_{Mo} is the accurately measured thickness of the Mo sample. Using the Rankine–Hugoniot equations, one can then determine pressure and density of Mo *absolutely* (e.g., without needing a known pressure reference), enabling one to develop an EOS standard.

This platform will be extremely useful to all programmatic activities interested in EOS and Hugoniot measurements at pressures of tens of Mbar, where currently there are no materials whose EOS has been experimentally determined.

This campaign built upon the results obtained in the past fiscal years. Very good quality data [Fig. 25(b)] were obtained in all 14 shots, also thanks to improvements in the target fabrication procedure that allowed us to obtain many planar targets and therefore more-accurate measurements of the shock velocity.

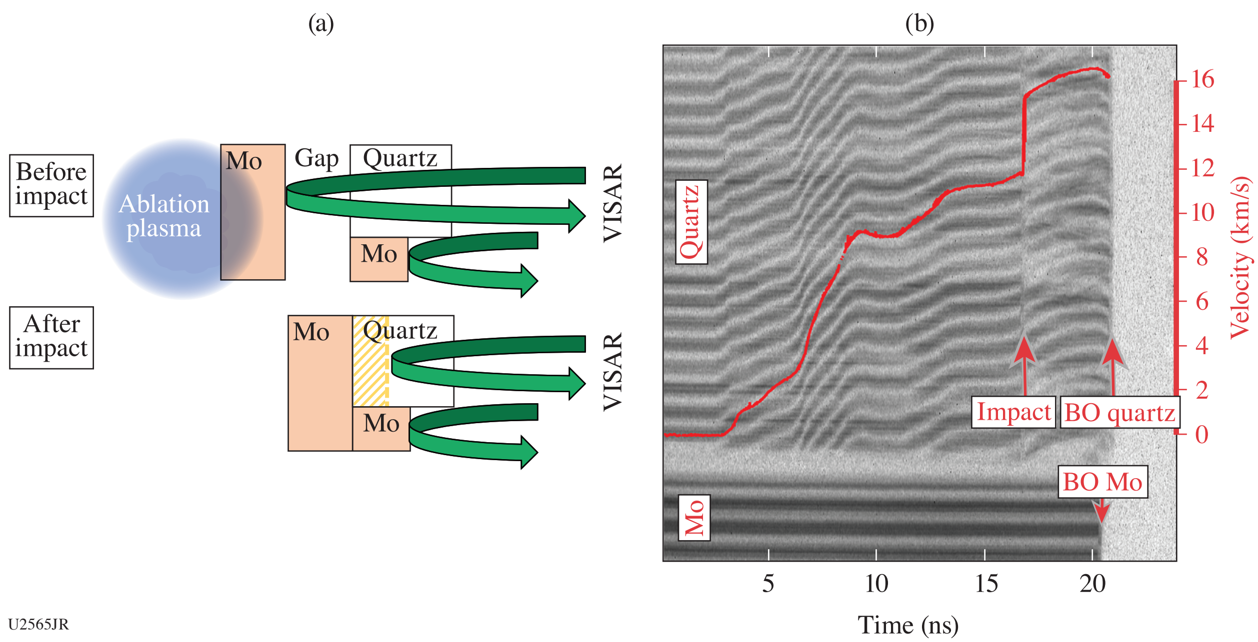

Figure 25
(a) Schematic representation of the experimental setup. A Mo foil is accelerated across a vacuum gap and impacted on a transparent quartz window, mounted side-by-side to a Mo foil. The simultaneous measurement of the flyer velocity and shock velocity upon impact with VISAR gives a measurement of the Mo EOS, without the need to rely on the EOS of a reference material. (b) Representative VISAR record. The main events are indicated by arrows.

The Mo EOS was explored up to U_s =16 km/s corresponding to about 12 Mbar. In-depth data analysis will allow us to determine if this platform represents a viable path toward absolute EOS measurements.

Developing a Conically Convergent Platform for Measuring Hugoniot Equation of State in the 100-Mbar to Gbar Pressure Regime
Principal Investigator: A. E. Lazicki
Co-investigators: F. Coppari, D. Swift, R. London, D. Erskine, H. Whitley, and J. Nilsen

This campaign was designed to develop a platform for measuring Hugoniot EOS of arbitrary (including high-Z) materials at pressures much higher than can be achieved using a standard planar drive. This platform is intended to collect data in the >100-Mbar pressure regime, where currently very little data exist for any material, for the purpose of constraining EOS models. To achieve the desired pressure amplification, we launched converging shock waves into a plastic cone inset in a halfraum. For appropriate cone angles, nonlinear reflections of the shock wave result in the formation of a Mach stem: a planar high-pressure shock that propagates along the axis of the cone.

Previous OMEGA shot days from FY16–FY19 tested design concepts in preparation for shots on the NIF. We have not previously been able to generate a Mach wave on OMEGA with sufficient steadiness, planarity, and surface area to perform an EOS measurement of sufficient accuracy because of limitations in pulse energy and length, but we have successfully tested the effects of a wide range of optimization concepts, including cone material, height and angle, hohlraum size and gas fill, laser pulse length and energy, and various schemes for heat shielding.

The shots in FY19 (3 half-days for a total of 20 shots) were specifically aimed toward testing a new scale of hohlraum (0.85-mm length, 1.15-mm diameter) midway between the standard, larger-scale EOS hohlraum (1 × 1.3 mm), which produced insufficiently supported Mach waves, and a smaller scale (0.7 × 1 mm) tested in FY18, which resulted in supported Mach waves but with insufficient surface area, and very high levels of hard x-ray preheat, presumably from hohlraum laser–plasma instability (LPI). We also tested a new concept for constraining target preheat levels by measuring time-resolved x-ray fluorescence, pumped by the hohlraum radiation, from a thin layer of Cu placed in contact with the physics package.

The mid-scale hohlraum produced Mach waves with a slightly reduced area compared to the large-scale hohlraum, but they were better supported, steadier, and more planar. We generated pressures up to ~180 Mbar in an Au stepped target, over an ~170-μm planar area (Fig. 26). We also tested the effects of changing Mach cone angle in the mid-scale hohlraum and can clearly

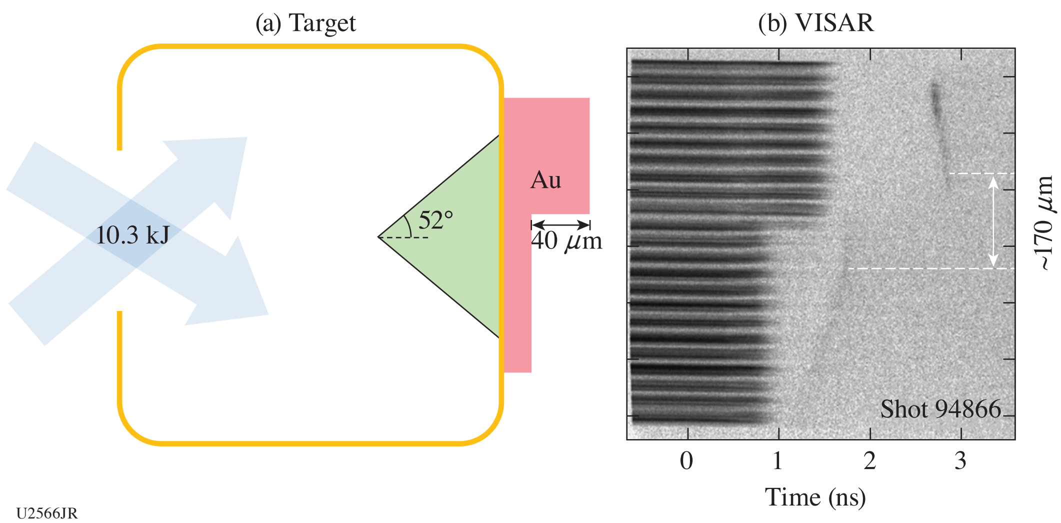

Figure 26
Mach wave generated in a CH cone and propagated through an Au stepped target. Average shock speeds of ~36.4 km/s were achieved in the Au. The VISAR reflectivity is lost about 1 ns before the shock wave breaks out, indicating that the free surface of Au melted. Shock-wave breakout is indicated by a flash of light from thermal emission.

confirm a predicted trend toward higher Mach wave pressure and smaller area with decreasing cone angle. Because of the large columnar volume of very high pressure material generated in a Mach cone, on shot days 19A and 19B we tested the Mach cone as a neutron generator by making the cones out of deuterated plastic. We generated up to ~2×10^8 D–D yield with a pure CD cone and an order of magnitude lower when a CH ablator was deposited on the CD cone.

Liquid–Ice VII Phase-Transition Kinetics in Ramp-Compressed Water
Principal Investigator: M. C. Marshall
Co-investigators: M. Millot, D. E. Fratanduono, and R. F. Smith

RampWaterEP-19A studied the liquid–ice VII phase transition in ramp-compressed water at ultrahigh strain rates (>10^6 s^{-1}). The principal isentrope of water crosses the liquid–ice VII equilibrium phase boundary at ~2.5 GPa; however, ramp-compression experiments at the Sandia Z machine observed the phase transition at 7 GPa (Ref. 16). We are testing the metastability limit of liquid water by ramp compressing over ~10× higher compression rates than the Z experiments.

We completed one day on OMEGA EP with a total of 13 target shots. A shocked CH reservoir released across a vacuum gap and isentropically loaded the water cell shown in Fig. 27(a). A thin water layer (~15 μm), created using a sapphire diving board inside the water cell, was ramp compressed to ~15 GPa. The experiments were designed to observe two signatures of the phase transition using VISAR: The first was a stress release on the rear sapphire window of the thin water layer caused by volume collapse during the transition (ice VII is 60% more dense than liquid water). The second was a coincident dip in transmission through the water layer from optical scattering of the coexisting liquid and ice phases with different refractive indices.

Preliminary analysis suggests that freezing occurred in several shots at pressures ranging from 7 to 9 GPa. An example of the stress-release signature of freezing is shown in Fig. 27(b). No clear evidence for transient opacity has been identified. Analysis is ongoing, and a follow-up campaign that uses a variety of windows (sapphire, quartz, and PMMA) on the thin water layer is scheduled on OMEGA EP in FY20. Data will be compared to predictions using SAMSA, an LLNL kinetics code.

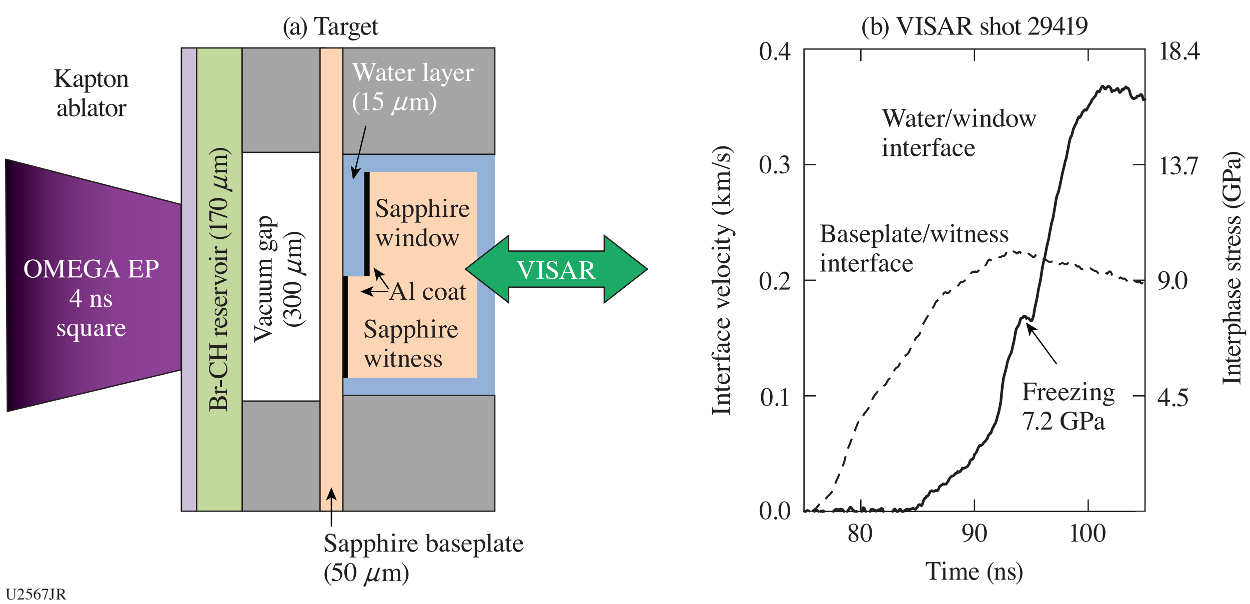

Figure 27
(a) Target design for a stress-release measurement and (b) interface velocity and stress as determined from VISAR. The velocity of the baseplate/Al/witness interface (dashed curve) provided a drive measurement for each target shot. The stress release on the water/Al/window is indicative of freezing (solid curve).

EXAFS Measurements Using Foil Backlighters and a Focusing Spectrometer
Principal Investigator: Y. Ping
Co-investigators: F. Coppari, A. Krygier, J. McNaney, and J. H. Eggert

In previous OMEGA shots, we discovered that foil backlighters are brighter than the implosion backlighter at x-ray energies >10 keV. This series of shots demonstrated the feasibility of EXAFS measurements using foil backlighters and a focusing spectrometer, and the results supported the associated NIF design.

The experimental setup is shown in Fig. 28. The foil backlighter (Ti, Ag, or Au) was irradiated by ~20 beams marked as green and pink in Fig. 28. The main target was a Fe foil sandwiched between diamond plates, mounted in a 3-D–printed plastic enclosure with a VISAR mirror and shield. For high-pressure shots, the Fe package was driven by five beams (blue) stacked in time to simulate a ramp drive. The focusing spectrometer was an imaging x-ray Thomson spectrometer (IXTS) with a toroidal crystal for 1-D spatially resolved x-ray spectra in Johann geometry, where the resolution is insensitive to the x-ray source size.

The Fe EXAFS spectrum was observed as shown in Fig. 29(a). The resolution was lower than expected due to an unexpected error in the radius of curvature of the toroidal crystal. In FY20 the position of the detector inside the IXTS will be adjusted to

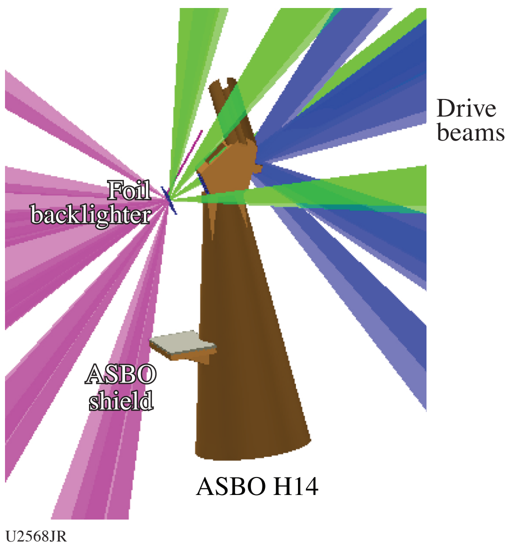

Figure 28
Experimental configuration.

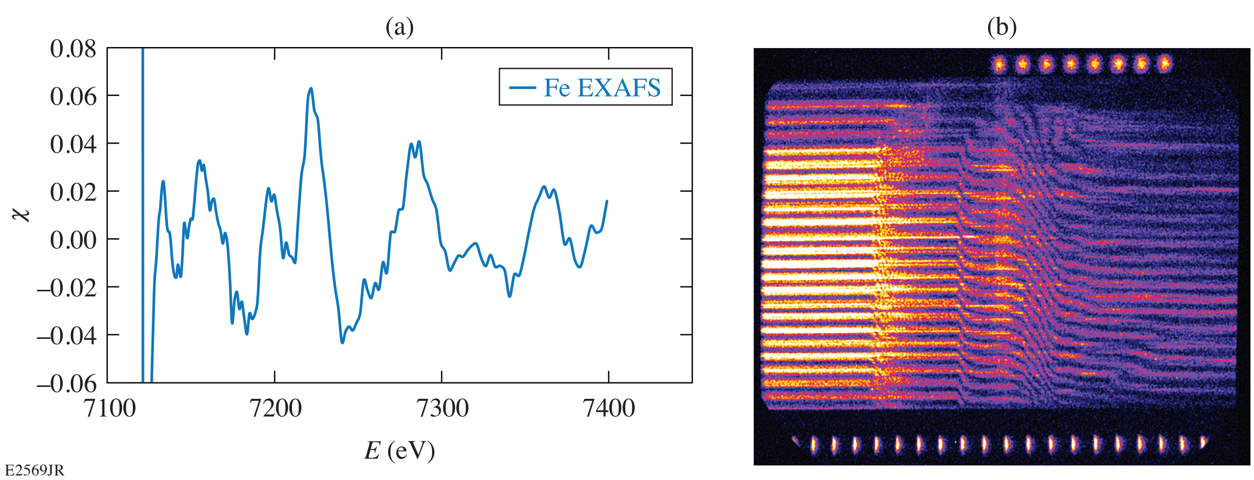

Figure 29
(a) Fe EXAFS spectrum from the IXTS with a Ti foil backlighter and (b) VISAR data for an ~5-Mbar drive.

match the actual radius of the crystal to improve the resolution. VISAR measurements were also demonstrated for the first time simultaneously with EXAFS measurements on OMEGA by adding a shield to block the direct line of sight from the backlighter to the ASBO lens as shown in Fig. 28. A typical VISAR raw image is displayed in Fig. 29(b). In comparison to prior implosion backlighters, foil backlighters require fewer laser beams and produce more photons above 10 keV. The new focusing geometry provides much higher signals on the image plate detector, providing a promising platform for x-ray absorption spectroscopy measurements.

Backlighter Development for EXAFS Measurements at High Energy on the OMEGA Laser
Principal Investigator: F. Coppari
Co-investigators: A. Do, Y. Ping, A. Krygier, and J. McNaney

EXAFS measurements require a bright, smooth, broadband x-ray source. X-ray radiation emitted by a capsule implosion meets these requirements and is currently used in laser-based EXAFS experiments. The x-ray emission decays quickly, however, at higher energies, making EXAFS measurements above 10 keV very challenging. For high-quality, higher-energy EXAFS measurements, there is a need for different x-ray sources. The bremsstrahlung radiation emitted by laser-irradiated higher-Z materials has the potential to be successfully used as such an x-ray source, provided the loss of spectral resolution in the measured EXAFS spectra due to source size effects can be mitigated. This can be accomplished by either collimating the x rays using a slit (although this will also reduce the total flux) or using a focusing spectrometer to measure the EXAFS signal.

During our two half-day campaigns we collected a total of 14 shots where we looked at different backlighter materials [Ti, Ag (including Ag foams), Au, Ge], varied the laser-drive conditions, and characterized the spectra in a wide energy range using combinations of different spectrometers (the flat x-ray Rowland spectrometer[17] and the dual-crystal spectrometer[18]).

We found that (1) the brightest spectra were measured for laser irradiance of the order of 10^{17} W/cm^2 and (2) Ti emits the brightest spectrum in the energy range below 25 keV, after which Au becomes brighter. Ti represents, therefore, a promising choice as a backlighter for EXAFS measurements at energies higher than 10 keV, where its spectrum is smooth and free from line emissions (see Fig. 30). A combination of a Ti foil backlighter and a focusing spectrometer is expected to significantly improve the EXAFS platform on the OMEGA laser and represents the point design for the development of the EXAFS diagnostic on the NIF. This configuration will be tested further during the next fiscal year on OMEGA.

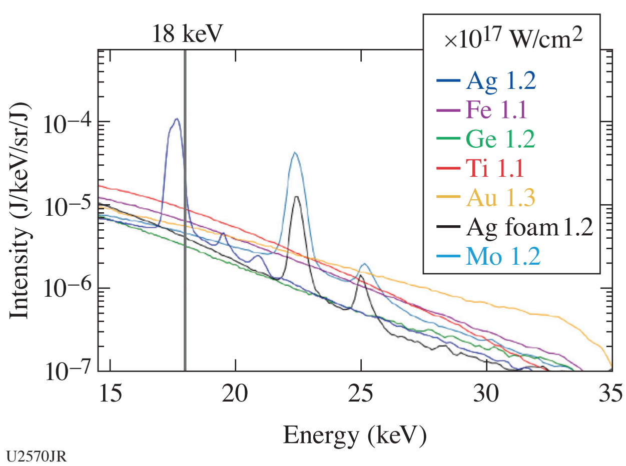

Figure 30
Spectra measured with the dual-channel spectrometer (DCS) for the backlighter materials studied in this campaign (also including data obtained on Ag and Mo in 2016) for laser irradiation of the order of 10^{17} W/cm^2. Our data clearly show that Ti is brighter than any other material looked at in this study for energies below 25 keV.

Isentrope Measurements of Isochorically Heated Materials
Principal Investigator: A. Saunders
Co-investigators: Y. Ping, A. Jenei, H. Whitley, J. Nilsen, and J. H. Eggert (LLNL); and M. Hill (AWE)

The aim of this new series of shots is to measure the release isentrope of heated materials. The isochoric heating was achieved by fast proton beams generated by high-intensity short laser pulses as illustrated by Fig. 31. The primary diagnostics are streaked

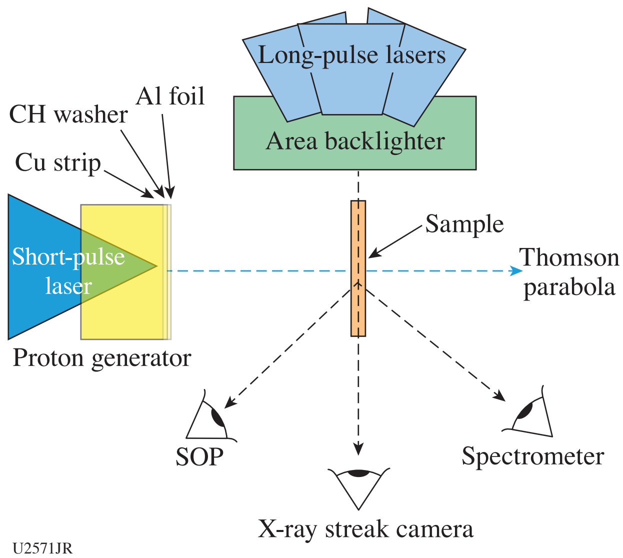

Figure 31
Experimental configuration.

x-ray radiography for time-resolved density profiles and SOP for initial temperature after the fast heating. The pressure is obtained from the density measurements using an analytical method developed by Foord *et al*.[19] The target was a 50-μm-sq ribbon of diamond, CH, or Al to allow radiography and SOP along two orthogonal axes. Other diagnostics, such as Thomson parabola and soft x-ray spectrometer VSG, were also fielded to provide the energy spectra of the proton beam and x-ray fluorescence spectra of the heated sample.

High-quality data have been obtained from both primary diagnostics as shown in Fig. 32. The x-ray radiograph clearly shows the expansion of the target. The SOP shows that there is some preheat by the x-ray backlighter, which was reduced in the second shot day by increasing the distance between the backlighter and the sample. Detailed data analysis is underway, and a paper on this new platform has been written for submission to Review of Scientific Instruments. Figure 32(c) shows two isentropes from two different EOS's: L130 and *SESAME* 3718 for Al at 2 eV. The large discrepancy between the two models, especially at lower densities, indicates a strong need of experimental data in this warm-dense-matter regime.

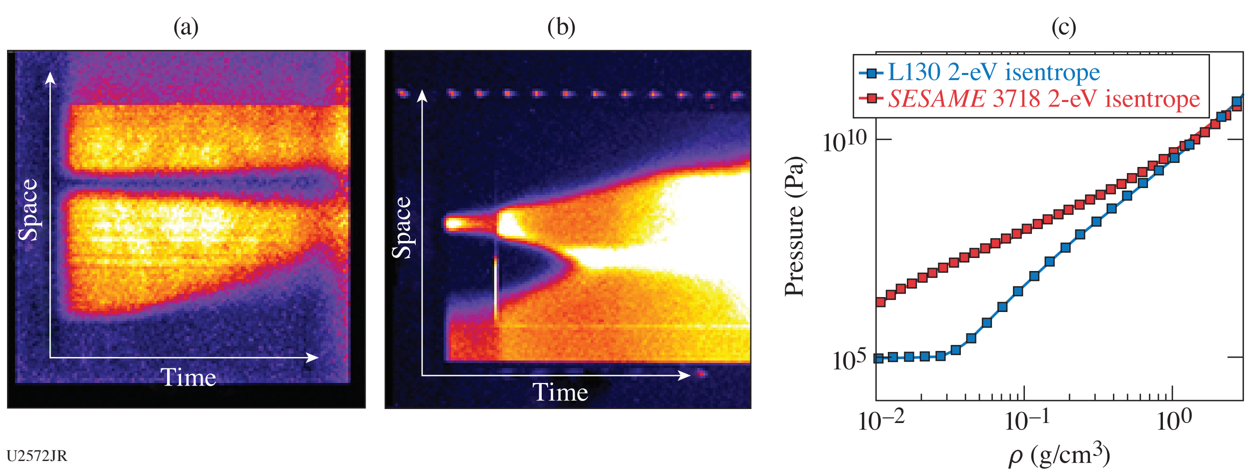

Figure 32
Streaked x-ray radiograph for (a) Al, (b) a SOP image, and (c) two isentropes from two EOS models: L130 and *SESAME* 3718 for Al heated to 2 eV.

Measurements of the Single-Crystal TATB Hugoniot to 80 GPa
Principal Investigator: A. Fernandez Pañella
Co-investigators: M. Marshall,* T. Myers, J. H. Eggert, T. Bunt, L. Lauderbach, and L. D. Leininger
*Postdoc

The purpose of the HEEOSEP-19A Campaign was to complete the Hugoniot measurements (initiated in FY18) of TATB (triamino-trinitrobenzene) shocked to a high pressure. TATB is a high explosive known for its insensitivity to high temperatures and impacts. Experiments were done on the OMEGA EP laser, where TATB was shocked to a range of pressures (15 to 80 GPa) over eight shots, filling up the gaps from the previous campaign. Hugoniot data were obtained by impedance matching relative to an aluminum standard. Planar targets had a Kapton ablator, aluminum base plate (standard), single-crystal TATB sample, and LiF witness used to correct for shock unsteadiness. Two laser beams with total energies of 580 to 2300 J were stacked in time, producing a 20-ns drive to support a nearly steady shock in the TATB. VISAR was used to measure interface velocities and shock transit times needed for the impedance-matching analysis. These results have been used to complete the single-crystal Hugoniot measurements of TATB (shown in Fig. 33). A manuscript has been written about these two campaigns.

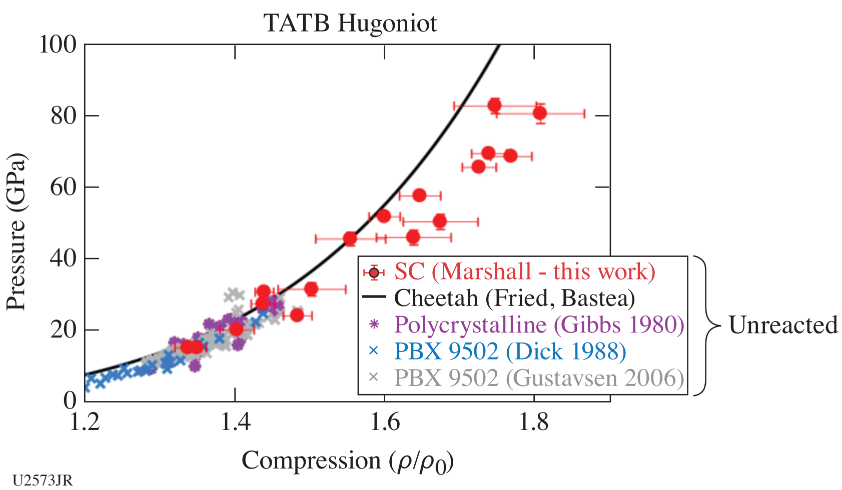

Figure 33
Single-crystal TATB Hugoniot. Pressure versus compression in a pressure range from 15 to 80 GPa covering unreacted and overdriven states.

Phase Transformations and Chemical Reaction in Shock-Compressed TATB
Principal Investigator: M. C. Marshall
Co-investigators: A. Fernandez Pañella, M. G. Gorman,* T. Myers, B. Yancey, J. H. Eggert, and L. D. Leininger (LLNL); and D. N. Polsin (LLE)
*Postdoc

The purpose of the HEXRDEP-19A campaign was to measure phase transformations and chemical reaction products in shocked TATB (triamino-trinitrobenzene) using x-ray diffraction. TATB ($C_6H_6N_6O_6$) is an insensitive high explosive that chemically reacts into inert gases and solid carbon species.

Experiments were done on the OMEGA EP laser, where TATB was shocked to pressures ranging 10 to 90 GPa over eight shots. The planar targets had an epoxy ablator, single-crystal TATB sample, and a Ti-coated LiF window mounted on a tungsten pinhole. Two laser beams with total energies of 190 to 1090 J were stacked in time, producing a 20-ns drive to support a nearly steady shock in the TATB. The two remaining beams were incident on a Fe backlighter foil, producing He$_\alpha$ emission to probe the crystal structure of the shocked TATB. X-ray diffraction data were obtained using the PXRDIP diagnostic, and VISAR was used to measure the TATB/LiF interface velocities needed to determine the shocked TATB pressure.

Initial results indicate that the TATB single crystals remain highly textured solids to ~40 to 50 GPa. A change in the x-ray diffraction pattern is observed when TATB is shocked over ~55 GPa. A new powder line, consistent with diffraction from the

(111) plane of diamond, is observed at 90 GPa (Fig. 34). Analysis is ongoing and a follow-up shot day using higher-energy Cu backlighters is scheduled for FY20. Data will be used to improve predictive modeling of chemical reactions in TATB-based explosives.

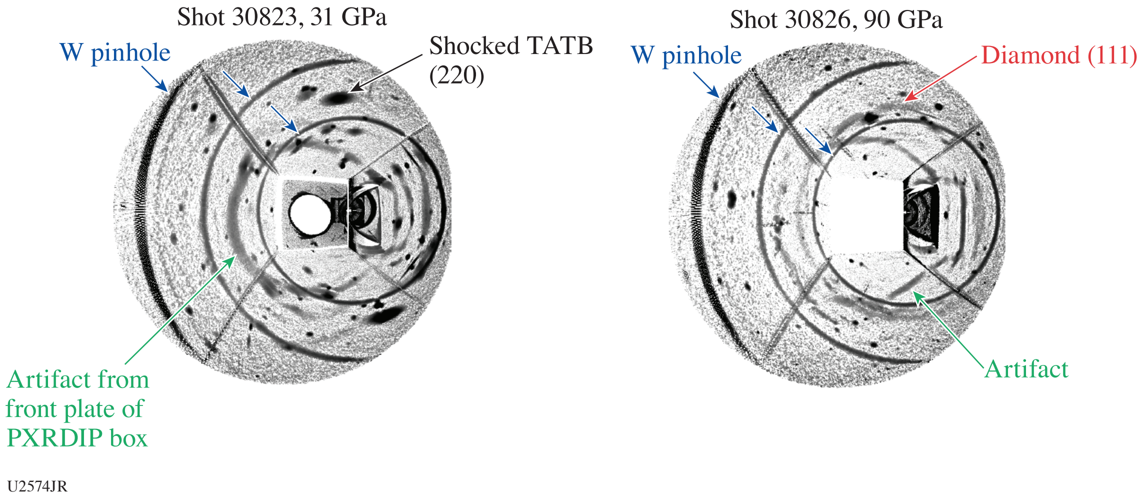

Figure 34
Stereographic projections of PXRDIP data for two shots.

3. Material Dynamics, Strength, and Ejecta Physics

Strength Experiments Using Direct-Drive Rayleigh–Taylor (DDRT) Growth Rates
Principal Investigator: A. Zylstra
Co-investigators: H.-S. Park, C. Stan,* D. Swift, T. Lockard, and J. McNaney (LLNL); and M. Hill and P. Graham (AWE)
*Postdoc

This campaign consisted of two OMEGA EP shot days with a total of 11 shots. The goal of this campaign is to measure the growth of pre-imposed ripples at a Rayleigh–Taylor (RT) unstable interface on a material sample of interest. Since the material strength will suppress the RT growth rate, strength in the HED regime can be inferred from the measured growth rate.

New in FY19 is the use of a direct-drive configuration on OMEGA EP, unlike previous indirect-drive strength experiments performed on OMEGA[20] or the NIF. The major advantages of a direct-drive platform are twofold: first, the pressure history on the sample can be changed by modifying the pulse shape, unlike the indirect-drive technique, which requires modifications to the target (through the "reservoir"); second, a direct inference of the growth rate can be performed by comparing the rippled sample in both driven and undriven regions.

The experimental configuration is shown in Fig. 35. Three long-pulse UV beams (2, 3, and 4) with 1.8-mm phase plates are used to drive the physics package. The beams are staggered in time to create a 30-ns drive using individualized and stitched pulse shapes to compress the sample to ~1 Mbar. The physics package is placed 14 mm toward TIM-12, which holds the primary diagnostics. For the RT growth measurements, the sidelighter beam shoots a microflag or microwire target placed 5 mm away from TCC to create a high-energy x-ray point-projection backlighter. The sidelighter uses 1000 J of energy in a 100-ps pulse. This campaign starts out using VISAR as the primary diagnostic to measure the shock propagation through a surrogate physics package, which characterizes the drive and sample conditions; then the diagnostic is switched to the LLNL Laue diffraction imager for radiography.

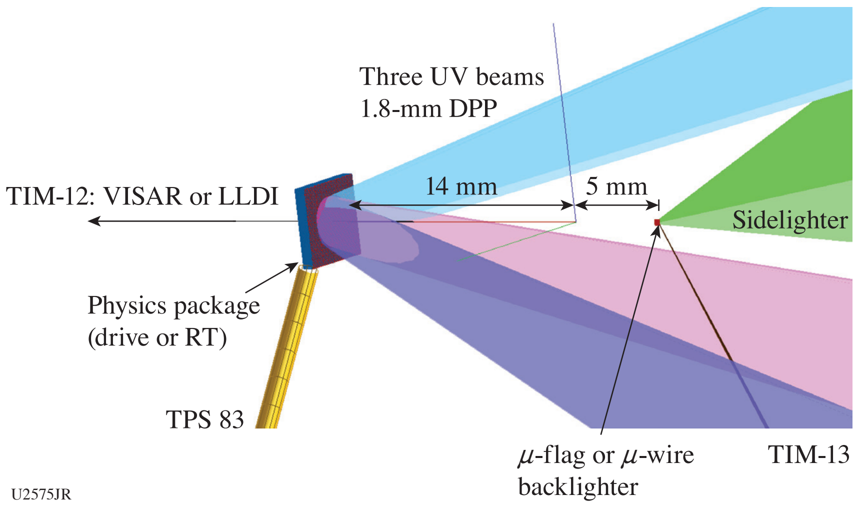

Figure 35
Experimental configuration.

The first shot day, DDRT used tantalum as the material to enable comparison to Ref. 20 and develop the platform. Excellent radiography data were obtained; the results are being interpreted and prepared for publication. Sample radiographs are shown in Fig. 36. Initial indications are that the new analysis method enabled by the direct-drive platform can substantially reduce the uncertainties associated with the strength growth factor measurements. On the second day, the material was switched to tin. An example radiograph is also shown in Fig. 36. Measuring the strength of tin at HED conditions will provide data needed for a tri-lab project on material strength. Good data were obtained early in time; at the latest sample times, the data appear compromised by instability growth at a Au/Re preheat shield layer between the ablator and the tin sample. Data analysis is still in progress, and the platform will be adapted for improved measurements in FY20 toward meeting the tri-lab goals.

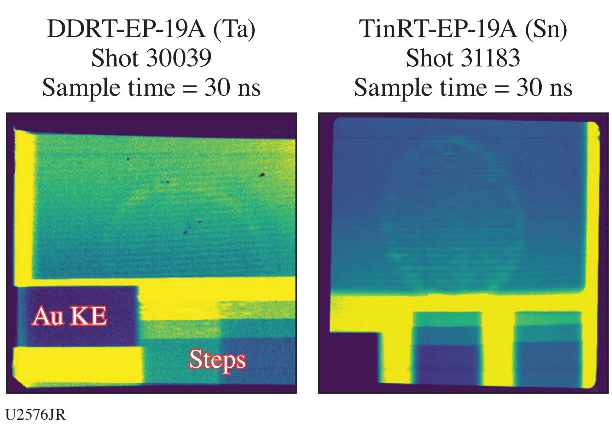

Figure 36
Raw radiographs from each shot day; the growth factor analysis and interpretation is in progress.

Spall and Recollection in Ramp-Compressed Tin

Principal Investigator: S. J. Ali

Co-investigators: A. Saunders, H.-S. Park, J. H. Eggert, A. Fernandez Pañella, F. Najjar, T. Haxhimali, B. Morgan, Y. Ping, and C. Huntington (LLNL); and H. G. Rinderknecht (LLE)

In dynamically compressed materials undergoing ductile failure, the formation and coalescence of voids due to high-rate tensile stress induce spallation—the formation of one or more 2-D sheets that detach from the bulk material. Eventually, the material behind the sheets may catch up and recollection can occur, potentially resulting in the closure of the voids or fractures and, depending on the mechanical response of the material, healing of the surface. The formation and recollection of spall layers is a leading hypothesis to explain the origin of spatially heterogenous reflectivity loss and recovery observed in-line VISAR results for free-surface dynamic compression experiments. In ramp-compression experiments on polycrystalline tin on the NIF with small initial shock, this reflectivity loss and late-time recovery are observed in free-surface experiments where the initial shock is below the bct to bcc phase transition, as shown in Fig. 37, but no longer observed when the initial shock is higher. This suggests that the reflectivity loss is due to damage and breakup of the surface during spallation, and that the subsequent impact of either additional spall layers or the bulk, as indicated by the observed acceleration of the material, contributes to the healing or repair of the observed surface. To determine the microphysical nature of the damage, it is necessary to resolve both the spatial distribution of the ejected material fragments and their velocities.

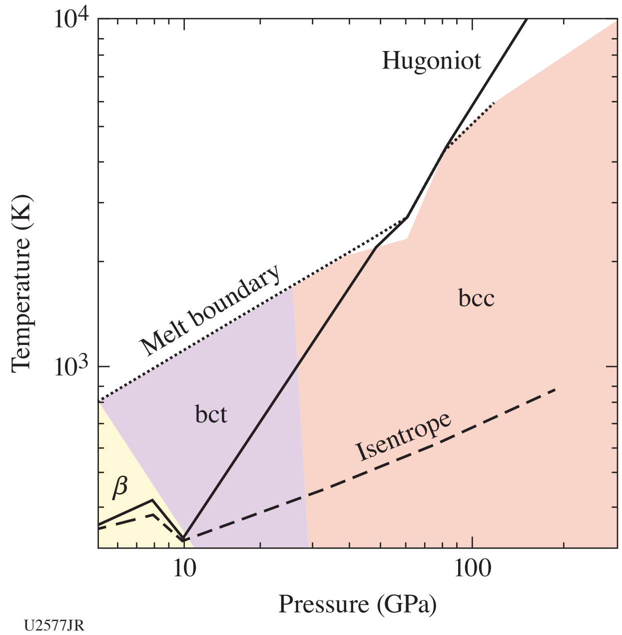

Figure 37
Tin phase diagram.

We used the OHRV, a 2-D velocimetry diagnostic, to simultaneously image and measure the velocity of ramp-compressed tin. Over the course of two half-day campaigns, we were successful in smoothly ramp compressing tin to a peak pressure of 50 to 100 GPa, through the bct–bcc phase transition. While we observed spall-like behavior, shown in Fig. 38, and fracture along grain boundaries, we did not observe the reflectivity recovery and acceleration seen in NIF experiments. Ramp compression was accomplished using a plasma-piston drive, which allows for less flexibility in pulse shaping; and our current hypothesis is that the behavior observed in the NIF experiments is more sensitive to drive than initially suspected. Further work will be required to understand this sensitivity.

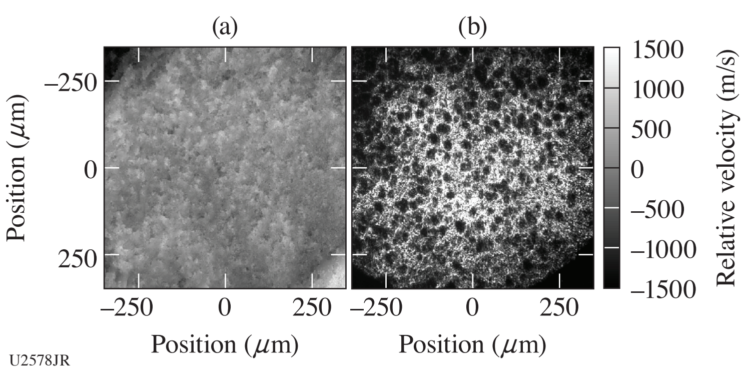

Figure 38
OHRV results from a shot ramping tin to ~70 GPa. An OHRV probe was on compression at ~50 GPa. Both (a) a velocity map and (b) an image show round features indicative of solid material spall.

Development of High-Power Laser Platforms to Study Metal Ejecta Interactions

Principal Investigator: A. Saunders
Co-investigators: S. J. Ali, H.-S. Park, J. H. Eggert, F. Najjar, T. Haxhimali, B. Morgan, Y. Ping, and C. Huntington (LLNL); and H. G. Rinderknecht (LLE)

High-velocity ejecta and dust grain interactions are of great interest to the Stockpile Stewardship Program as well as interstellar and interplanetary science. Ejecta particles are generated by the Richtmyer–Meshkov (RM) instability when a strong shock wave interacts with surface defects while breaking out at a metal interface into vacuum or gas. Ejecta formation has been studied extensively, but ejecta particle transport, interaction, and recollection are still poorly understood. This project has been working to apply to this topic novel experimental techniques and diagnostics that have been developed for high-energy laser studies. Specifically, we have used x-ray radiography, as well as 1-D and 2-D VISAR to explore the details of ejecta transport, interaction, and recollection.

We developed a platform for the OMEGA laser to measure the areal mass density emerging from surface perturbations on tin foils. The platform uses the previously developed target fixture designed to make concurrent 1-D and 2-D VISAR measurements, allowing us to quantify the conditions in the tin upon shock release and provide data about the areal mass density of the ejecta jets. The target package is shown in Fig. 39(a) and consists of an ablator, a tin sample with multiple divots, and a silicon-nitride collection plate. The silicon nitride is 100 nm thick and reflects a fraction of visible light such that it provides a reflective surface for the VISAR measurements. Jets emerging from the tin divots impact on the silicon nitride window, causing it to accelerate. One-dimensional VISAR measures the motion of the silicon nitride and tracks the velocity as a function of time. Through the equations for momentum conservation, one can solve for the areal mass density of the ejecta jets in terms of the velocity of the SiN window.[21] The 2-D VISAR provides an image of the jets impacting the SiN, as well as the velocity as a function of position, as shown in Fig. 40.

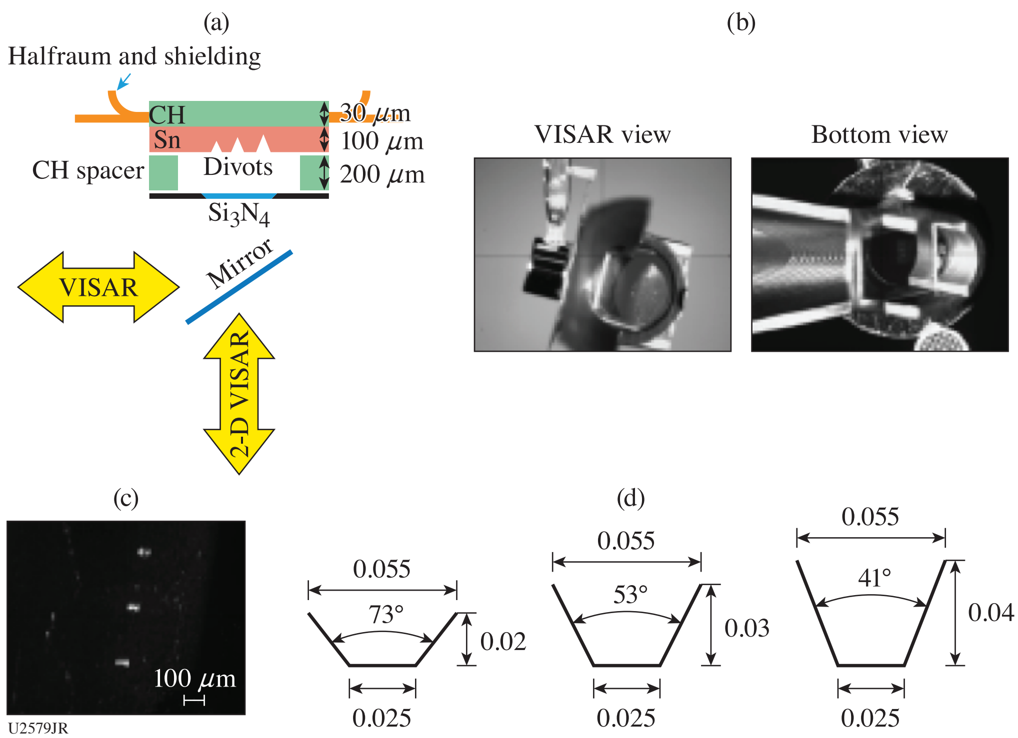

Figure 39
(a) Target schematic; (b) photos of the actual target from the 1-D VISAR view and the bottom view; and (c) image of the divots on the tin surface; and (d) divot schematics.

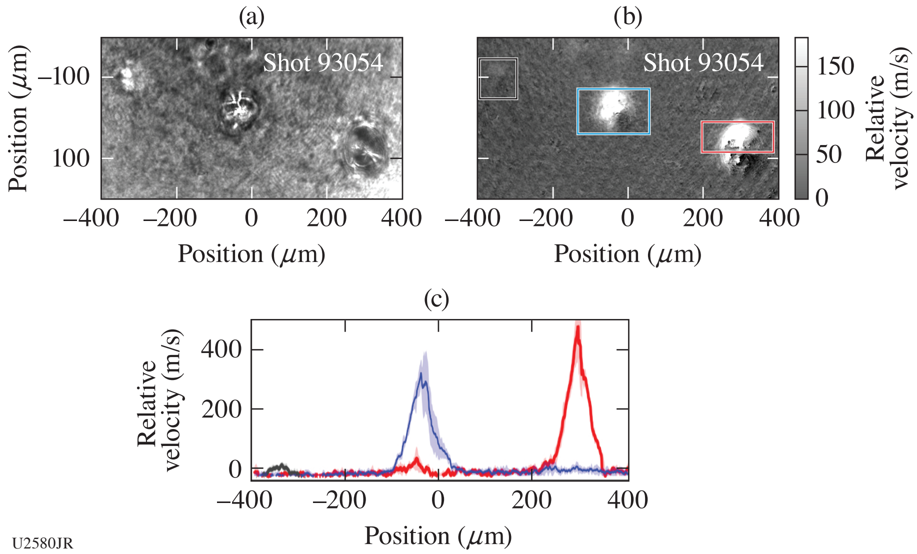

Figure 40
Two-dimensional VISAR results from one ejecta shot with three divots with varying depths showing (a) an image of the ejecta interacting with the SiN, (b) velocity of the ejecta/SiN interaction, and (c) lineouts of the velocity for each divot.

Study of Metal Ejecta Recollection, Interactions, and Transport on OMEGA EP

Principal Investigator: A. Saunders

Co-investigators: H.-S. Park, S. Ali, J. H. Eggert, T. Haxhimali, K. MacKay,* B. Morgan, F. Najjar, Y. Ping, and C. Stan* (LLNL); H. G. Rinderknecht (LLE); and P. Tzeferacos (University of Chicago)

*Postdoc

This campaign consisted of three shot days with a total of 27 shots to develop a laser-driven experimental platform to understand ejecta properties, especially during their recollection, interactions, and transport processes. Ejecta are submicron to micron particles that can travel at hyper velocities (1 to 10 km/s). Understanding ejecta interactions has broad relevance to many fields of science including impact material physics and debris shielding.

In FY19, the OMEGA EP Ejecta-Interact Campaigns focused on creating ejecta in both solid and liquid stages, measuring their jet velocities, and developing a radiography platform to understand their morphology and evolution. Figure 41 shows the experimental configuration. The target was a 30-μm-thick ablator with a 100-μm-thick Sn metal foil. The Sn had a long 45-μm-

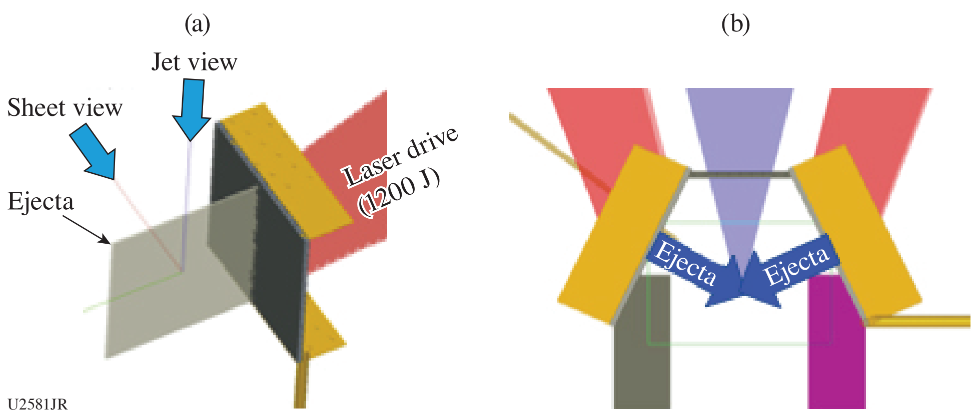

Figure 41
Experimental configuration: (a) single jet platform; (b) interacting jet platform.

deep groove with a 60° opening in the middle of the surface. The laser drive shocks the Sn target. Release of the shock onto the free surface generates RM instabilities from the surface perturbation, and ejecta jets are created. Figure 41(a) is the platform for the single jet and (b) is the interacting jet configuration.

The drive used 1.8-mm-diam phase plates and an 8-ns square pulse with varying laser energies. We tried three different laser energies to control the ejecta phase (i.e., liquid and solid.) The drive was measured by the VISAR diagnostic on separate shots. From the free-surface velocity measurements, the particle velocities were calculated. From these particle velocities, using the well-known Hugoniot EOS table for Sn, the shock velocities and the shock pressure were derived. The ~1120-J laser energy resulted in an ~100-GPa shock pressure that was well above the Hugoniot melt line; therefore, the ejecta were in the liquid state. At ~300 J, we measured ~42 GPa, which is still in the liquid state; at ~70 J, we measured a shock pressure of ~16 GPa, which is well below the melt line. These drive calibration shots were crucial to understanding the ejecta state.

For radiography, we used the short-pulse–driven Ti microwire backlighter that generates predominantly 4.5-keV K_α x-ray photons with ~10-μm spatial resolution. The target geometry was varied such that the radiography was viewing two different orthogonal angles, the "jet" view and "sheet" view of the ejecta jet. Figure 42 shows the resulting single ejecta jet evolution from both jet and sheet view radiography. For these shots, we used a 1200-J drive that created melted Sn ejecta at ~100-GPa shock pressure. The initial analysis indicates that the ejecta jet velocity was ~5.3 km/s; the bulk surface was ~2.5 km/s. The radiometric data show that the areal mass density was ~0.3 mg/cm^2 (Ref. 21). The ejecta front travels at a faster velocity than the bulk surface of the tin that can be seen preceding the bulk surface in the radiography.

For the EjectaInteract-EP-19C Campaign, we created solid-state Sn ejecta jets using ~70 J of drive laser energy that delivered ~16 GPa of shock pressure. Figure 43 shows the resulting radiography in the jet and sheet views. The sheet view shows interest-

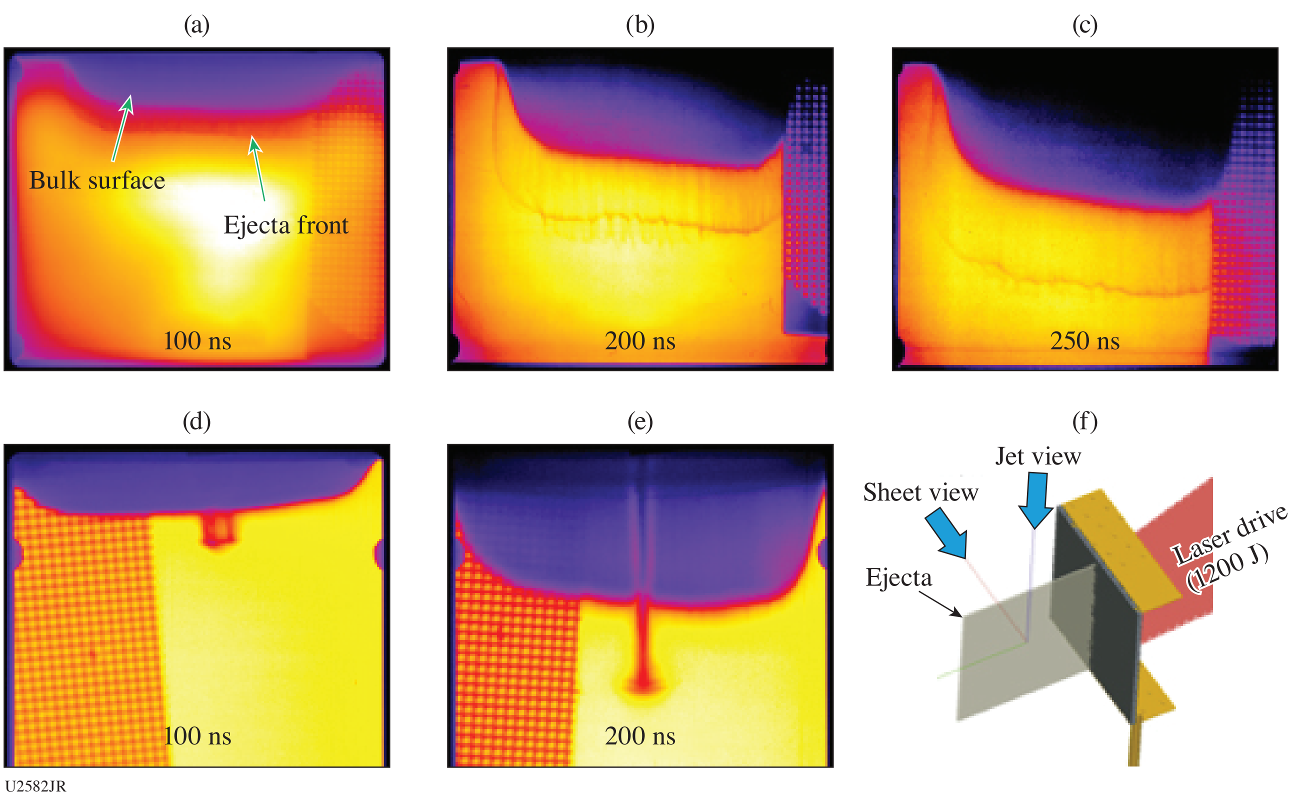

Figure 42
Raw radiographs of expanding liquid Sn ejecta jets taken at different delay times. The top row is the "sheet" view; the bottom row is the "jet" view.

ing layered features that could be spalling. From these views, the solid Sn ejecta jet velocity is ~2 km/s. The interacting jets are created by shocking two targets in opposite directions. The interacting jet view is shown in the third panel. The lineout of the interacting region shows more obscuration of the signal, indicating that the ejecta density was piling up from inelastic scattering.

Future campaigns will study more details of the interacting ejecta properties and the effect of different materials and different groove shapes. In addition, particle-plate interactions will be studied.

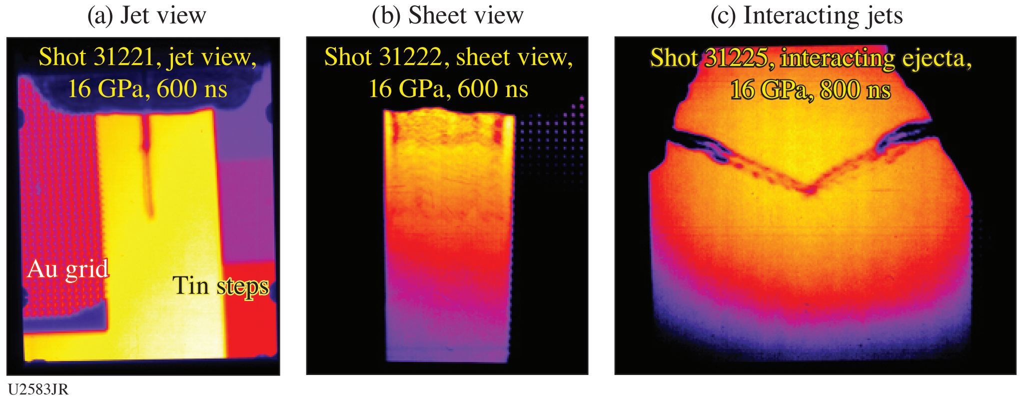

Figure 43
Raw radiographs of expanding solid Sn ejecta jets with (a) "jet" and (b) "sheet" views. (c) The interacting jets are created by two opposing targets. Density pile-up was observed in the interaction region.

4. National Security Applications

SolarCellESD: Solar Cell Electrostatic Discharge Experiments
Principal Investigator: K. Widmann
Co-investigators: P. Jenkins and J. Lorentzen (NRL); S. Seiler (DTRA); and J. Emig, P. Poole, and B. Blue (LLNL)

To determine experimentally whether prompt x rays can induce failure modes in solar arrays remains the key goal of the SolarCellESD Campaign. The main difference in vulnerability of an array compared to a single solar cell is the presence of a voltage difference between neighboring cells that can be up to hundreds of volts depending on the overall layout of the array. For the experiments on OMEGA, we continue to field the smallest-possible array, i.e., 2 × 1 cells with electronic controls that allow us to dial in a voltage difference (bias voltage) between the two cells and, therefore, to study the failure modes as a function of incident x-ray flux and bias voltage, respectively.

For the FY19 campaign we deployed a new solar cell coupon design, with a new mechanical support structure that made it easier to exchange the solar cell coupons between shots. We continued using the electromagnetic interference (EMI) enclosure, but fielded two of the four Langmuir probes in the "shadow" of the EMI enclosure, i.e., away from the line of sight of the incident x rays (see Fig. 44). The goal of this arrangement was to investigate if the Langmuir probe signal is partly generated by a possible x-ray–induced blow-off plasma from the solar cells. Measurements from the probes in the shadow showed no significant signal above the noise level and, therefore, validated our interpretation of the signal from the Langmuir probes that remained in the line of sight of the x-ray source.

We were able to bracket the threshold conditions for the onset of an electrostatic discharge and for the development of sustained arcing for a fixed bias setting. We observed significant variation, however, in the breakdown response based on the view angle for the azimuthally asymmetric laser drive (azimuthal with respect to the hohlraum axis). This important finding will determine the geometry of the experimental setup for upcoming SolarCellESD Campaigns. We also tested a high-temperature hohlraum rather than halfraum as the x-ray source. Unfortunately, a failure of the Dante gate valve prevented us from measuring the performance of this new x-ray source, but we plan to repeat the test of the new source in FY20.

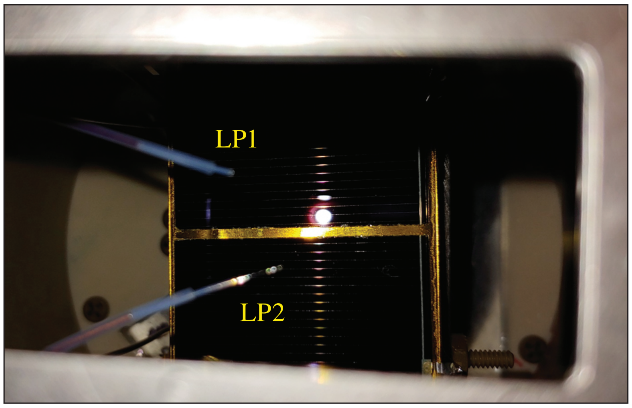

U2584JR

Figure 44
View of the gap between the two solar cells of the 2 × 1 mini array as seen through the aperture of the EMI enclosure. The two features on the left (LP1, LP2) are the Langmuir probes that are in the line of sight of the x-ray source. These probes are several centimeters above the surface of the solar cells.

Plasma-Instability Control to Generate a High-Energy Bremsstrahlung X-Ray Source
Principal Investigator: P. L. Poole
Co-investigators: R. Kirkwood, S. C. Wilks, M. May, K. Widmann, and B. E. Blue

FY19 continued a campaign to develop a high-fluence x-ray source in the 30- to 100-keV range by optimizing plasma instabilities. High-fluence sources at lower energies are currently used for materials effects studies in extreme environments, but no good source exists for >30-keV x rays. This project aims to enhance laser conversion to plasma instabilities like stimulated Raman scattering (SRS) and two-plasmon decay (TPD), which accelerate electrons in plasma waves that will convert to high-energy x rays via bremsstrahlung in the high-Z hohlraum wall.

Two half-day campaigns during FY19 attempted to optimize and prolong the duration of plasma conditions that have been found favorable for strong plasma-wave generation. Experiments from previous years demonstrated x-ray yield enhancement from two hohlraum fills (inner CH liner and low-density CH foams) that also enhanced different plasma instabilities and therefore different components of the x-ray spectrum. A natural evolution for FY19 was to study these effects in combination: the insets in Fig. 45 show the usual Au hohlraum with 1-μm-thick CH "windows," which could be ablated by the initial prepulse just like the inner liner, but this redesign allowed CH foam to be fielded as well between the windows to maintain sufficient plasma density as the laser ablated away material. This design was also fielded with foam layers increasing in density toward the center of the

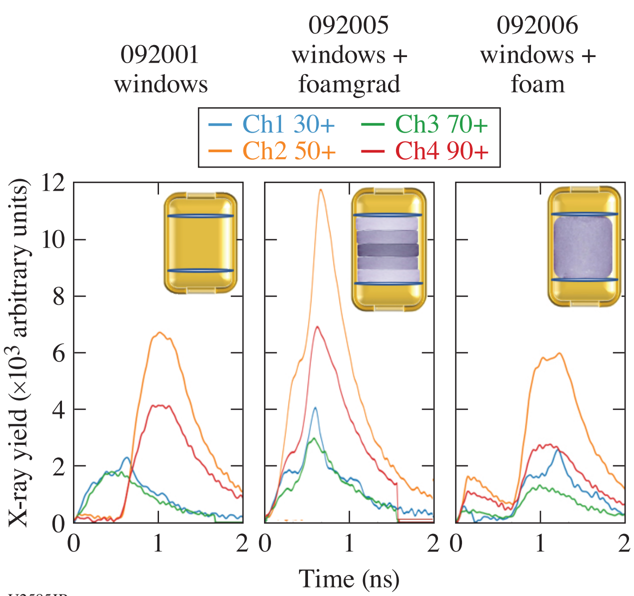

U2585JR

Figure 45
Hard x-ray detector signal from three shots (target type indicated by inset). Enhancement of the desired >50-keV channel (orange curve) is observed for the windowed hohlraums, with further increases (factor-of-4 integrated yield) for the windowed, layered foam hohlraums.

hohlraum. Hard x-ray detector signals (Fig. 45) showed enhancement of the desired >50-keV x rays (orange) with the CH window designs and a further 4× enhancement in total yield for targets that also contained the foam layers.

The results from the OMEGA campaign were used to design a complementary NIF shot day in Q2 FY19, which demonstrated an increase in the hot-electron temperature distribution and thereby the >50-keV hard x-ray signal over FY18 results. These successes have enabled the first shots of materials in high-fluence, hard x-ray environments on the NIF and are being fielded on more campaigns in FY20, even as optimizations continue. This new x-ray source represents a large capability increase for national security applications and related materials under extreme condition studies, with the additional benefit of broadening the understanding of plasma instability control for fusion and other applications.

Enhancing Multi-KeV Line Radiation from Laser-Driven Nonequilibrium Plasmas Through the Application of External Magnetic Fields

Principal Investigator: G. E. Kemp

Co-investigators: D. A. Mariscal,* P. L. Poole,* J. D. Colvin, M. J. May, and B. E. Blue (LLNL); A. Dasgupta, A. L. Velikovich, and J. Giuliani (NRL); and C. K. Li and A. Birkel (MIT)

*Postdoc

A recent LLNL Laboratory Directed Research and Development effort (17-ERD-027) has been studying the influence of externally applied magnetic fields on laser-driven x-ray sources—like those typically used for high-fluence radiography or backlighters—with the ultimate goal of improving multi-keV x-ray conversion efficiency through thermal transport inhibition. The goal of this series of shots was to test and qualify a platform for fielding externally generated magnetic fields on previously fielded x-ray sources on the OMEGA laser. This platform is intended to collect data in the 20-T magnetic-field regime, where currently very little data exist for such high-Z, non-LTE (local thermodynamic equilibrium), magnetized plasma conditions. The collected data will be used to constrain thermal transport inhibition and MHD models currently used in the multi-physics radiation-hydrodynamic code *HYDRA*.

The experimental configuration is illustrated in Fig. 46. Thin-walled, cylindrical Kr gas pipes (1.5 atm) were driven by 20 kJ of laser energy in a 1-ns pulse (40 beams) as typical sources of ~13-keV K-shell line radiation. A total of six shots were taken, half of which had externally imposed B fields. A dual-MIFEDS design was adopted to reach ~20-T field strengths (compared to ~13 T from MagXRSA-18A). Quantifying changes in x-ray emission with increasing external B-field strength was the primary goal of the shots, recorded with Dante (0 to 20 keV), hard x-ray detectors (20 to 500 keV), pinhole cameras (>2 keV), and the DCS (11 to

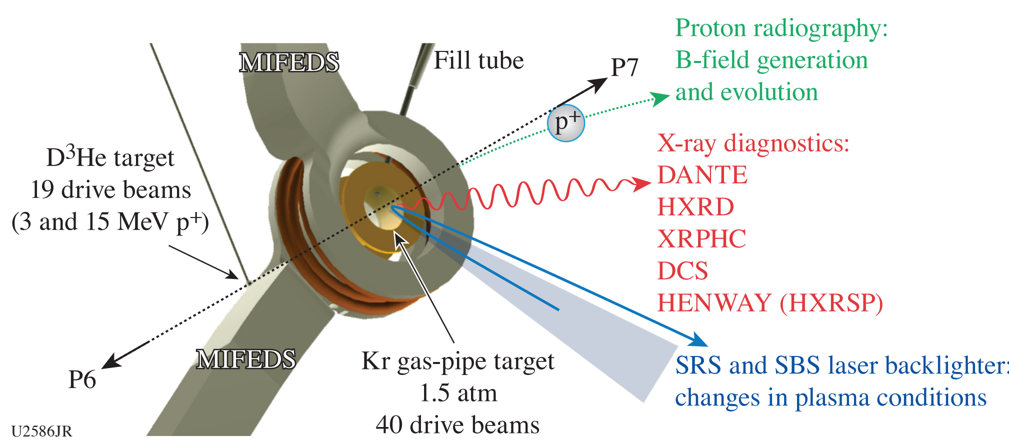

Figure 46
Experimental configuration for MagXRSA-19A. X-ray emission, laser backscatter, and proton radiography data were simultaneously obtained to quantify the evolution and influence of external B fields in these interactions.

45 keV). Secondary diagnostics included proton radiography and stimulated Raman/Brillouin laser backscatter. A D^3He backlighter capsule provided a source of 3- and 15-MeV protons. Analysis is ongoing, but initial results suggest ~50% enhancements in multi-keV Kr emission (>8 keV) when the 20-T B field was present, consistent with the pre-shot modeling.[22] Enhancements of 2.6× were also observed in the >80-keV emission, suggesting B fields could also be used to enhance continuum emission.

Preliminary results from this campaign have led to additional shot time in FY20. With the recent MIFEDS hardware upgrades, we anticipate fields in excess of 40 T in the dual-MIFEDS configuration. These promising results have also justified parallel NIF platform development later in FY20, where we will explore magnetized Ag and Xe K-shell x-ray sources.

5. Plasma Properties

Development of a Platform to Benchmark Atomic Models for X-Ray Spectroscopy of Shock-Heated Materials
Principal Investigator: M. J. MacDonald
Co-investigators: A. M. Saunders, T. Döppner, C. M. Huntington, K. B. Fournier, H. A. Scott, and T. Baumann (LLNL); S. R. Klein, K. Ma, H. J. Lefevre, C. C. Kuranz, and E. Johnsen (University of Michigan); and R. W. Falcone (University of California, Berkeley)

The FoamXRFTS-19A Campaign was the second shot day to develop a platform using simultaneous x-ray fluorescence (XRF) spectroscopy and x-ray Thomson scattering (XRTS) to measure the equation of state of shocked foams. The goal of this platform is to provide XRF spectroscopy data from shock-heated materials at known temperatures, measured independently using XRTS, to benchmark atomic models for future XRF diagnostics.

This platform uses a planar shock wave to heat a cylinder of foam doped with a mid-Z element, similar to previous results published from the Trident Laser Facility at Los Alamos National Laboratory,[23] with the addition of an XRTS diagnostic. A laser-driven Zn He_{α} backlighter induced K-shell fluorescence from the Co-doped foam and also served as the x-ray source for XRTS. The IXTS spectrometer recorded spatially resolved Co K_{β} XRF, measuring the density profile of the shock wave in the foam in addition to resolving XRF spectra from the shocked and unshocked regions of the foam. This campaign successfully demonstrated the ability to measure Co K_{β} spectra from the shock-heated layer at a range of drive conditions, as shown in Fig. 47(a). Initial estimates of the peak temperature in the shocked layer from the Co K_{β} spectra as a function of drive energy are shown in Fig. 47(b). The temperatures are from simulated emission spectra calculated using Cretin,[24] an atomic kinetics and radiation code developed at LLNL. Although the XRTS data collected in these experiments will be difficult to interpret due to noise in the data, the results will be helpful in improving the experimental setup for future campaigns.

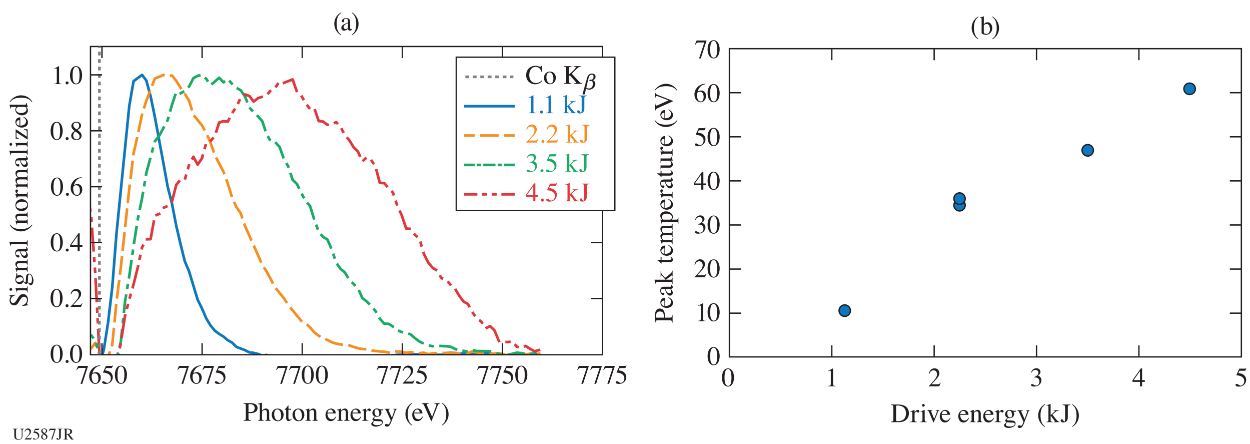

Figure 47
(a) Co K_{β} spectra taken at different drive energies after removing the contribution from unshocked material. (b) Peak temperatures in the shock-heated foam determined by fitting Co K_{β} emission to Cretin simulations.

Measurement of Au M-Shell Emission Using A Buried Layer Platform

Principal Investigator: E. V. Marley
Co-investigators: R. F. Heeter, M. B. Schneider, G. E. Kemp, M. E. Foord, D. A. Liedahl, K. Widmann, and J. Emig (LLNL); D. Bishel (LLE); and G. Perez-Callejo (University of Oxford)

This campaign was designed to measure the emitted M-shell gold spectra from a well-characterized and uniform plasma for comparison to atomic kinetic models. The buried-layer target geometry used for this experiment is capable of generating plasmas with an electron temperature of ~2 keV at electron densities of 10^{21} electrons per cubic centimeter. These are also the conditions found inside gold hohlraums used on experiments on the NIF, providing a stable laboratory setting for radiation transport and atomic kinetic studies.

Planar, buried-layer targets were illuminated equally on both sides [Fig. 48(a)] to heat the sample. The sample used in the campaign was a 1300-Å-thick Au/V mixture designed to burn through completely before the end of the laser pulse, providing uniform plasma conditions to measure the M-shell emission of the gold. The samples were buried between two 5-μm-thick layers of Be, which acted as an inertial tamp slowing the expansion of the sample. The targets were designed so that the sample would be concentric with the Be tamp. However, they were not laser cut to spec and only one of the targets had a sample concentric with its Be tamp.

Time-resolved 2-D images of the target's x-ray emission, viewed both face on and side on, were recorded using pinhole cameras coupled to framing cameras. The 4ω probe beam and Thomson spectrometer were also used to measure the scatter off of the electron and ion-acoustic features [see Fig. 48(b)]. A new filter package was used during the campaign to filter out the self-emission and unconverted light, which has been an issue in the past with high-Z targets, and good quality data were obtained. The K-shell spectra from V were used to determine the electron temperature of the plasma. The time-resolved spectra were recorded using a crystal spectrometer coupled to a framing camera. Two crystal spectrometers were used to record the full range of the Au M-shell emission, also time resolved. All of the framing cameras used, those for imaging as well as those for spectroscopy, were co-timed so the plasma conditions could be determined for the measured Au M-shell emission.

A single pulse shape was used during the campaign: a 3.0-ns square pulse with a 100-ps picket arriving 1 ns before the main pulse. A complete (all six diagnostics, correctly timed) set of data was recorded during the campaign at temperatures ~2 keV.

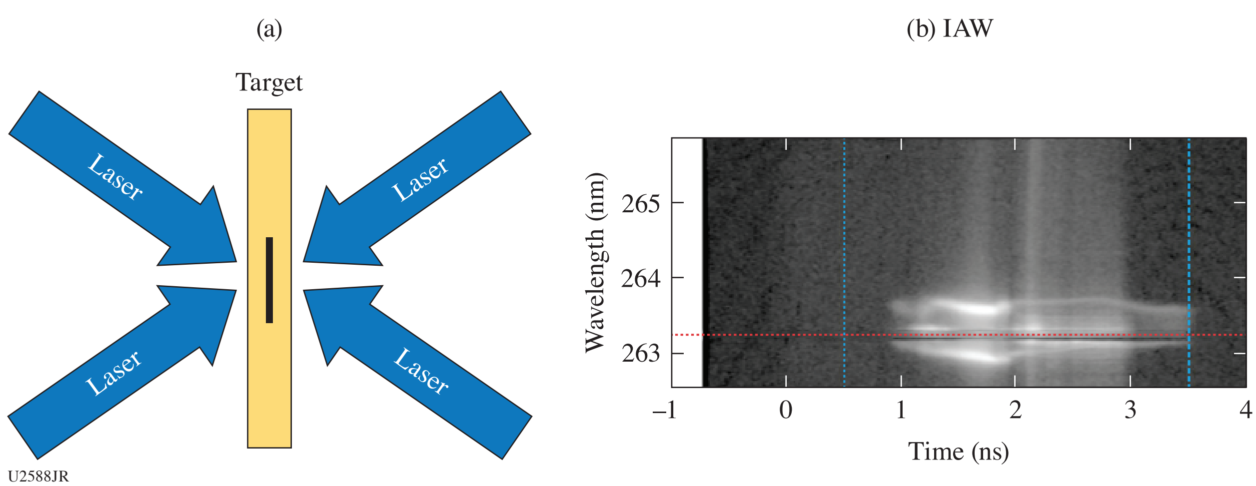

Figure 48
Experimental configuration and Thomson-scattering data of shot 93556.

6. Hydrodynamics

Performance Verification of Ta_2O_5 Foams for Hydro Experiments
Principal Investigator: D. A. Martinez
Co-investigators: M. Rubery and S. McAlpin (AWE); and S. Prisbrey (LLNL)

Foam targets are used on a variety of experiments on the NIF, and verification of the EOS of specific foams is necessary for accurate experimental design and analysis. In this experiment on OMEGA, we tested the Ta_2O_5 foam at a 0.85-g/cm^3 density over the course of five laser target experiments. The experiment consisted of a gold hohlraum heated with 15 drive beams with a 1-ns pulse at 360 J/beam. The heated hohlraum indirectly drove a polyimide ablator, which was used to simultaneously drive a quartz sample and a Ta_2O_5 sample. Using VISAR and SOP we can verify the drive on the plastic ablator using the quartz sample and use the information to calibrate our post-shot simulations so we can compare the shock breakout time of the Ta_2O_5 foam sample through an SOP measurement. Additionally, the Ta_2O_5 foam produced a reflecting shock while the shock was traversing through the Ta_2O_5, allowing the VISAR diagnostic to provide an additional measurement to verify the accuracy of our Ta_2O_5 equation-of-state tables. Figure 49 shows the velocity measurements inferred from the VISAR diagnostic. The Ta_2O_5 used the index of refraction reported from Miller.[25] The post-shot simulation results shown used only the laser drive to determine the shock velocity in the quartz. The experiments provided useful information for our team to calibrate our models for future NIF experiments.

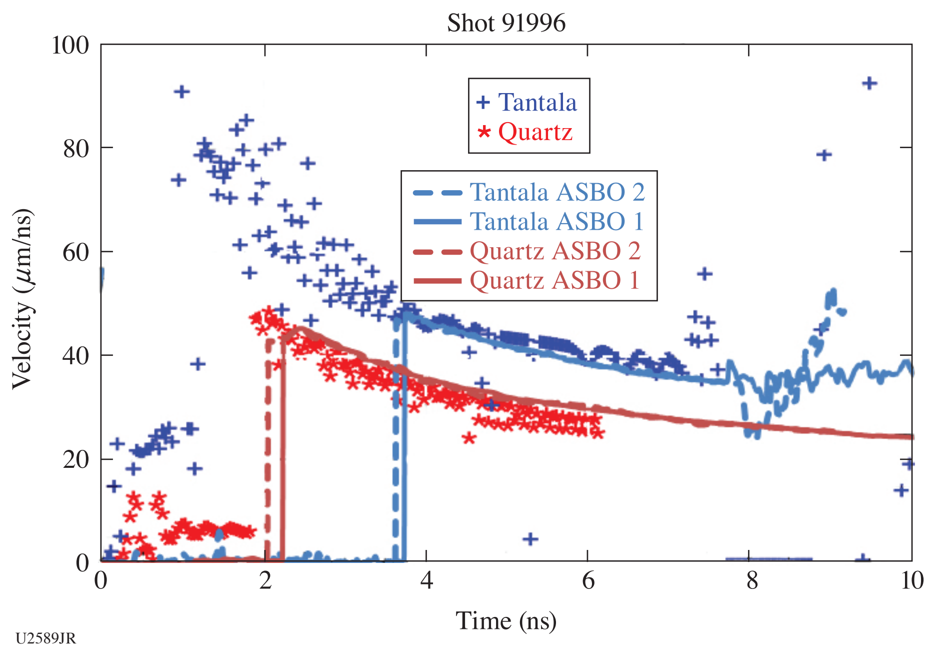

Figure 49
The measured velocity of the reflecting shock from the VISAR diagnostic. Both legs of the diagnostic are reported as active shock breakout (ASBO) 1 and 2.

Mitigating Crosstalk Between High-Energy Backlighters with Shielding
Principal Investigator: S. F. Khan
Co-investigators: D. A. Martinez, S. C. Wilks, S. Prisbrey, D. Kalantar, and A. J. Mackinnon

The objective of these OMEGA EP experiments is to test three shield designs to mitigate the cross interaction of a dual wire backlighter system with a long delay. Previous OMEGA EP experiments (Dbl-HEBL-18A) showed that fratricide between the wires significantly degraded the resolution of the second wire for delays above 4 ns. The experiments used two 12.5-μm-diam W wires with a separation of 4 mm. Shields between the wires consisting of gold (375 μm), plastic (500 μm), and their combination were tested. Each wire was illuminated by infrared 50-ps, 1-kJ short pulses with time intervals of 0, 10, and 15 ns. Source size of each wire was inferred by a radiograph of a gold test grid. Shadowgraphs of the second wire were recorded using the fourth-harmonic probe laser beam and qualitatively illustrates the expansion of the wire (see Fig. 50).

The tested shields show that for a 10-ns time separation, the source size of the second wire was essentially the same as the first wire within measurement uncertainties. Since the plastic shield is transparent to x rays above 10 keV, this indicates that the electrons or very soft x-rays from the initial wire are the primary mechanism for degradation. The results from this experiment are being used in backlighter development experiments on the NIF.

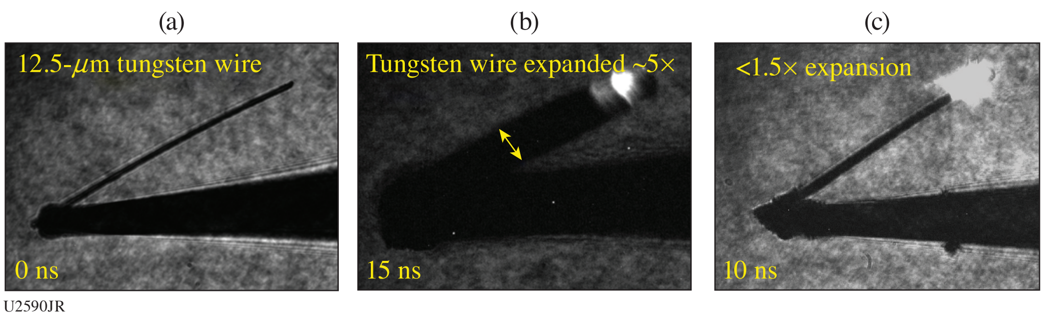

Figure 50
Shadowgraphs of the second wire using the fourth-harmonic probe beam. (a) The wire before either of the wires is illuminated; (b) the second wire 15 ns after the first wire was illuminated with no shielding in between; and (c) the second wire with a 500-μm polyimide shield in between the wires and 10-ns delay. The polyimide shield mitigates the expansion.

Broadband MeV Gamma-Ray Source Development
Principal Investigator: N. Lemos
Co-investigators: A. Pak, D. Rusby, J. Williams, and A. Mackinnon

Following 2011 OMEGA EP experiments,[26] we have begun to investigate the potential of laser-driven MeV radiography. A series of shots was designed to reproduce the past results using one OMEGA EP short-pulse beam and to improve those by coupling the two OMEGA EP short-pulse beams into the same target. We successfully reproduced the past results and showed an improvement when coupling the two beams into the same target.

This experiment had three objectives: (1) reproduce the results presented in Ref. 26; (2) study fratricide by separating both beams in space and time; and (3) maximize x-ray yield by overlapping both beams in space and time. The setup used to achieve the three objectives is shown in Figs. 51(a)–51(c), respectively. For all these configurations the laser beams had an energy of 900 J per pulse and a pulse duration of 10 ps, the electron beam temperature was measured, and a high-density object [image quality indicator (IQI)] was radiographed. The electron beam temperature was used to optimize the x-ray emission since it directly relates to the x-ray spectrum temperature,[27] and the IQI was used to characterize the x-ray source imaging capabilities.

Figure 52 shows the measured electron temperature for all three experimental setups. The highest electron temperature was achieved when overlapping both beams in time and space (green circle), i.e., maximum intensity on target. The second-hottest

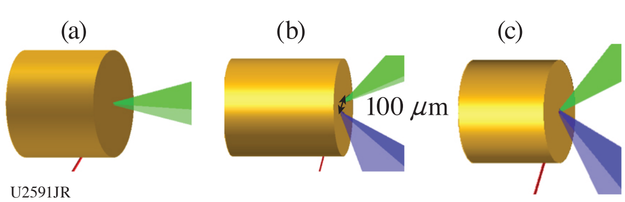

Figure 51
Three experimental setups used in this experiment.

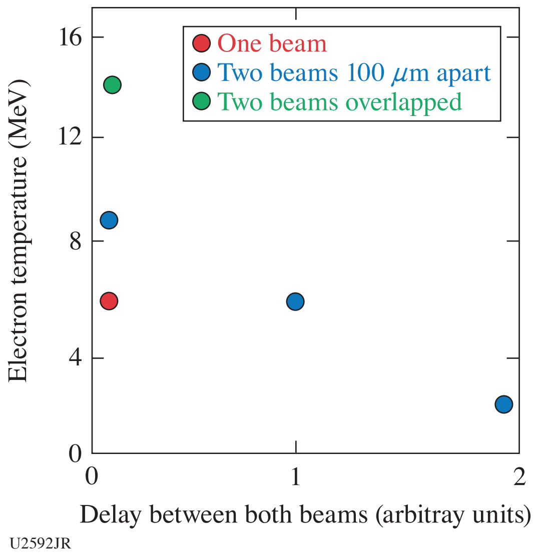

Figure 52
Electron beam temperature for the three experimental setups versus delay between both beams.

electron spectrum was achieved when both beams were separated by ~100 μm (blue circles) followed by the single-beam shot (red circle). To study fratricide we separated both beams by ~100 μm and delayed both beams up to 2 × 5 ns (blue circles). It is clear that when both beams are delayed in time, fratricide is occurring since the electrons' beam temperature starts to drop.

Figure 53(a) shows a CAD drawing of a section of the IQI, and Fig. 53(b) shows the highest-quality radiograph of the IQI with an areal density of 13 g/cm^2 obtained when using the experimental setup in Fig. 51(c). Here we summed the signal recorded in 12 image plates in order to increase the signal-to-noise ratio. Results of this campaign are being used to optimize a similar platform that is being developed on the NIF-ARC.

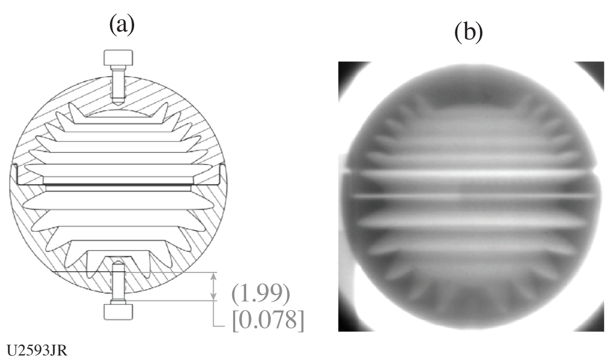

Figure 53
(a) CAD section of the IQI and (b) x-ray image of the IQI.

This work was performed under the auspices of the U.S. Department of Energy by Lawrence Livermore National Laboratory under Contract DE-AC52-07NA27344.

1. *LLE 1999 Annual Report, October 1998–September 1999*, 222, Rochester, NY, LLE Document No. DOE/SF/19460-332 (2000).
2. D. K. Bradley *et al*., Phys. Plasmas **16**, 042703 (2009).
3. D. K. Bradley *et al*., Phys. Rev. Lett. **102**, 075503 (2009).
4. S. W. Haan *et al*., Phys. Plasmas **18**, 051001 (2011).

5. J. H. Eggert *et al*., Nat. Phys. **6**, 40 (2010).
6. M. Millot, Phys. Plasmas **23**, 014503 (2016).
7. S. Le Pape *et al*., Phys. Rev. Lett. **120**, 245003 (2018).
8. L. X. Benedict *et al*., Phys. Rev. B **89**, 224109 (2014).
9. M. Millot *et al*., Phys. Rev. B **97**, 144108 (2018).
10. J. R. Davies *et al*., Phys. Plasmas **24**, 062701 (2017).
11. J. Kim *et al*., Phys. Plasmas **25**, 083109 (2018).
12. L. Burakovsky *et al*., J. Phys.: Conf. Ser. **500**, 162001 (2014).
13. P. C. Myint *et al*., J. Phys. Chem. Phys. **150**, 074506 (2019).
14. L. E. Kirsch *et al*., J. Appl. Phys. **125**, 175901 (2019).
15. J. K. Wicks *et al*., Sci. Adv. **4**, eaao5864 (2018).
16. D. H. Dolan *et al*., Nat. Phys. **3**, 339 (2007).
17. D. B. Thorn *et al*., Rev. Sci. Instrum. **89**, 10F119 (2019).
18. J. F. Seely *et al*., High Energy Density Phys. **3**, 263 (2007).
19. M. E. Foord, D. B. Reisman, and P. T. Springer, Rev. Sci. Instrum. **75**, 2586 (2004).
20. H. S. Park *et al*., Phys. Rev. Lett. **114**, 065502 (2015).
21. A. M. Saunders *et al*., Lawrence Berkeley National Laboratory, Livermore, CA, Report LLNL-PROC-783445 (2019).
22. G. E. Kemp *et al*., Phys. Plasmas **23**, 101204 (2016).
23. M. J. MacDonald *et al*., J. Appl. Phys. **120**, 125901 (2016).
24. H. A. Scott, J. Quant. Spectrosc. Radiat. Transf. **71**, 689 (2001).
25. J. E. Miller, "High-Pressure Equation-of-State of Porous-Ta_2O_5," Ph.D. thesis, University of Rochester, 2007.
26. C. Courtois *et al*., Phys. Plasmas **18**, 023101 (2011).
27. A. Compant La Fontaine, C. Courtois, and E. Lefevre, Phys. Plasmas **19**, 023104 (2012).